POLITECNICO DI TORINO

Master degree in Energy and Nuclear Engineering

Photocatalytic generation of hydrogen from cellulose

Master of Science thesis

Supervisors:
Massimo Santarelli, Department of Energy, PoliTo
Joydeep Dutta, Department of Applied Physics, KTH
Rafael Eduardo Guedez Mata, Department of Energy Technology, KTH

Candidate:
Stefano De Luca

Academic year 2021-2022

Abstract

Uncontrolled emission of greenhouse gases caused by consumption of fossil fuels has led to the urgent need to develop low-emitting energy technologies such as those exploiting renewable energies. In this context, hydrogen (H_2) represents an opportunity to enhance the development of such technologies, in light of the possibility to use it as an energy storage for non-programmable renewables, and for its potential to decarbonize key emitting sectors such as the transport sector. This study is therefore focused on photocatalytic generation of H_2 using cellulose as sacrificial agent, with the aim of valorizing renewable resources like solar energy and the chemical energy contained in an abundant biopolymer. The types of cellulose which are most suitable for this application were determined, and the influence on the rate of H_2 production of parameters like pH of the reaction medium, and concentrations of cellulose and photocatalyst was clarified. It was found that an acidic pH, a relatively high concentration of photocatalyst and a relatively low concentration of cellulose constitute the most advantageous configuration to maximize the performances. An estimation of the conversion efficiency from light energy to H_2 energy is provided, and the performances allowed by cellulose are compared to those allowed by more frequently used sacrificial agents. Finally, attempts to synthesize advanced photocatalysts with the aim of increasing the efficiency are reported.

Acknowledgments

Il ringraziamento più grande va alla mia famiglia: mamma, papà, Benedetta, i nonni e tutti gli altri. Se io sono Stefano, e se sono arrivato fino a questa tesi, è innanzitutto grazie a loro.
Grazie alle maestre Anna, Franca, Maria e il maestro Cammarano, per gli insegnamenti e le solide basi fornitemi che mi accompagneranno a vita.
Grazie ai miei amici d'infanzia e adolescenza, agli amici di Torino, e a quelli nuovi conosciuti a Stoccolma con cui tante avventure ho vissuto.
Grazie ad Ascea con il suo mare e i suoi tramonti, le lunghe passeggiate tranquille, la Fiumarella, le colline piene di ulivi da cui si vede Capo Palinuro in mezzo all'azzurro, i resti di quella che un tempo fu Elea, il cibo buono, l'aria di casa.
Grazie alla Svezia, coi lunghi inverni di ghiaccio che d'un tratto regalano una giornata di sole, felice e inaspettata, le foreste piene di laghi blu, le giornate estive infinite, le fattorie, le casette rosse di campagna con le luci alle finestre.

Nomenclature

Ag_3PO_4	Silver Phosphate
CB	Conduction Band
CdS	Cadmium Sulfide
CM cellulose	Carboxymethyl cellulose
DI water	Deionized water
g-C_3N_4	Graphitic Carbon Nitride
HCOOH	Formic acid
HMF	Hydroxymethylfurfural
HOMO	Highest Occupied Molecular Orbital
hTPA	Hydroxyterephthalate
LHCE	Light-energy-to-hydrogen-energy conversion efficiency
LUMO	Lowest Unoccupied Molecular Orbital
N-GQDs	Nitrogen doped graphene quantum dots
Na CM cellulose	Sodium Carboxymethyl cellulose
PEC	Photoelectrochemical cell
SDBS	Sodium Dodecylbenzenesulfonate
SHE	Standard Hydrogen Electrode
TiO_2	Titanium Dioxide
TPA	Terephthalic acid
TPES	Total Primary Energy Supply
VB	Valence Band
WO_3	Tungsten Oxide
ZnO	Zinc Oxide

Contents

1 Introduction

As a consequence of the industrial development of the last years, the world is witnessing an increase of the atmospheric concentration of CO_2 never recorded before. CO_2 is recognized as the main contributor to the increase of the global temperature, that, according to the Treaty of Paris, must be limited to +2 °C with respect to the pre-industrial level in order to avoid irreversible and catastrophic consequences [1]. The uptrend of the concentration of CO_2 is a direct consequence of the massive amount of fossil fuels consumed by humanity, that, despite all the efforts, still dominate the global energy mix [2]. Figure 1 shows how the atmospheric concentration of CO_2 varied over the years, recently exceeding, for the first time after the Mid-Pliocene Warm Period, the 400 ppm threshold [3]. Figure 2 shows instead the evolution of the Total Primary Energy Supply (TPES) of the world by energy source, still clearly dominated by fossil fuels.

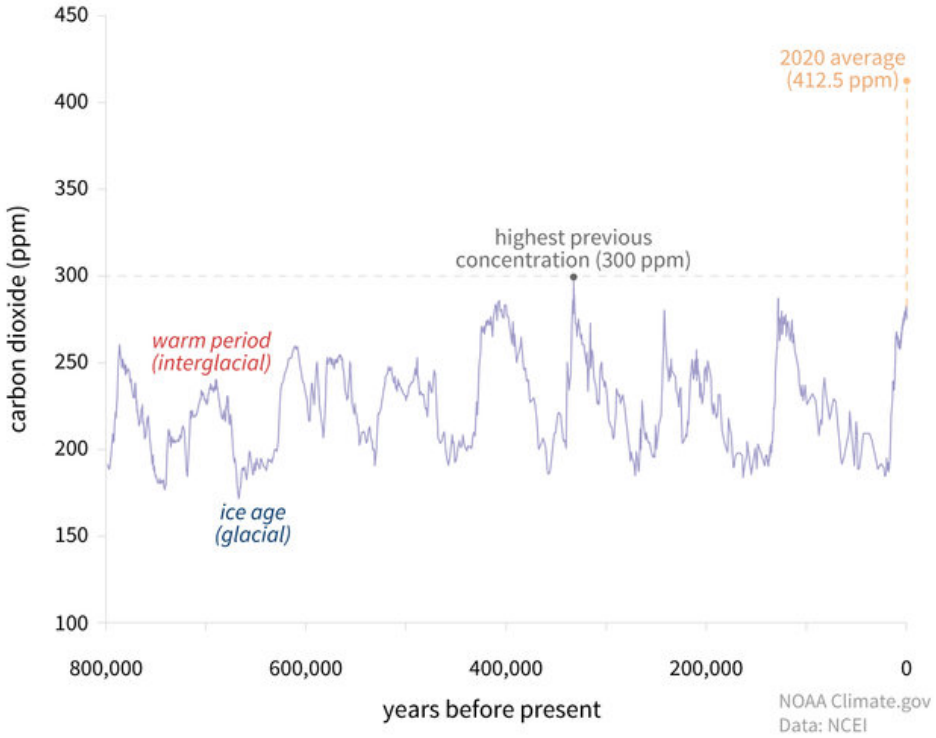

.

Figure 1: CO_2 concentration in the atmosphere in the last 800,000 years [3]

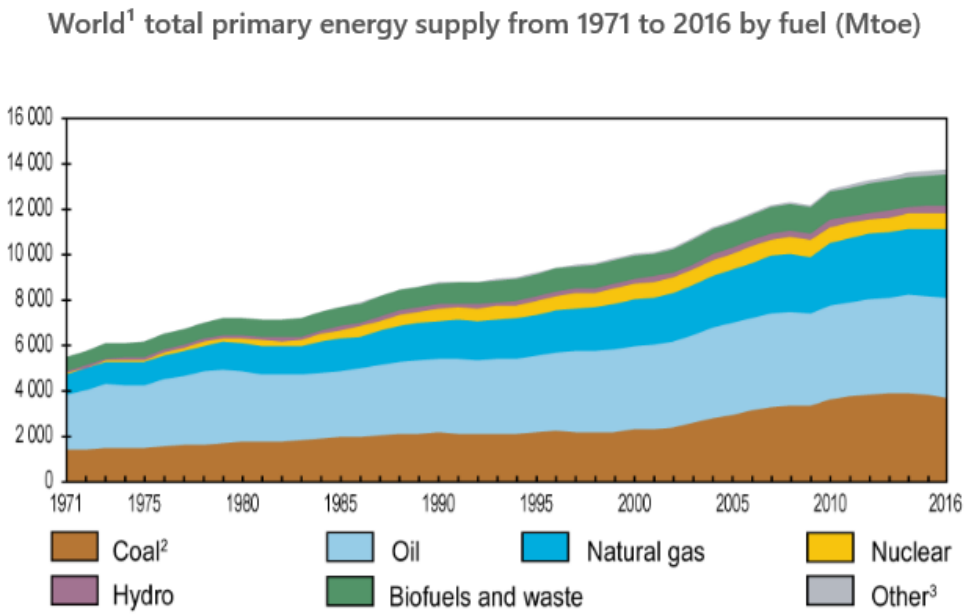

Figure 2: World TPES from 1971 to 2016 [2].

Substantial efforts have been done in the last years to reduce the emissions by switching to renewable energy sources. Renewables, however, mostly contributed to the decarbonization of the electricity sector, while the energy supply of other sectors such as the transport sector, is still largely covered by fossil fuels. As an example, it is possible to look at the Italian energy supply by source for electricity generation and transport for the same year (2014), shown respectively in Figure 3 and Figure 4.

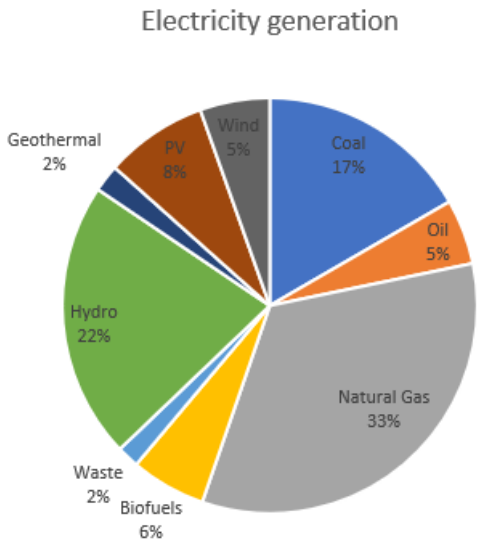

Figure 3: Italian energy supply for electricity generation by source (2014) [2].

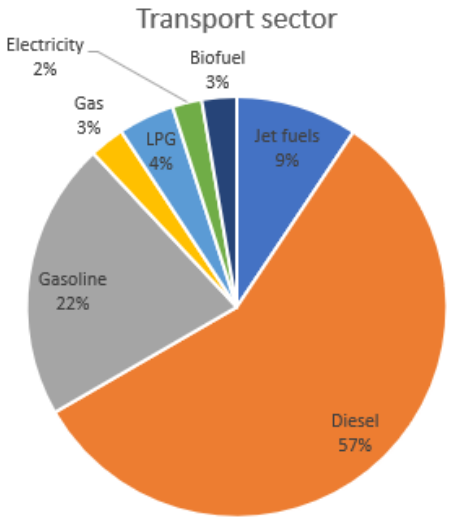

Figure 4: Italian energy supply for transport sector by source (2014) [4].

While low carbon sources account for almost half of the energy supply for electricity generation, the energy supply in the transport sector is almost completely based on fossil fuels. As a solution for the decarbonization of the transport sector, in recent years we have seen large investments in electric vehicles. A complete transition to electric vehicles may however be hindered due to a series of shortcomings. Huge investments are needed to upgrade the electric networks, with peak power that may double or triple in certain areas [5], and the toxicity of battery materials, whose improper disposal causes contamination of water, soil and air and constitutes a threat for organisms at various trophic levels [6]. An alternative to the electrification of the transport sector is the employment of H_2 as a fuel, that can be produced from renewable energy through clean processes like electrolysis, photocatalysis and solar thermochemical cycles [7]. The employment of H_2 would not be restricted to the transport sector, but would also be suited for electricity generation and heating/cooling purposes. H_2 would in addition constitute a way to store excesses of energy produced from non-programmable renewable sources such as solar and wind energy and to balance electrical and/or heating/cooling demands in moments of low production, making the energy distribution system as a whole more flexible [8]. In light of these considerations, this dissertation investigates the photocatalytic production of H_2 using cellulose as a sacrificial agent, being cellulose the most abundant biopolymer on earth [9].

The study is structured in the following sections: Section 2 provides a theoretical background about the physical principles underlying the process, while Section 3 reviews the previous advancements reported in literature and highlights what is still unknown. Based on the information gathered from literature, Section 4 proposes the research question that this work attempts to answer, while Section 5 clarifies the corresponding scope and lim-

itations. Section 6 specifies how the experiments were structured, and Sections 7 and 8 contain information about the photocatalyst material and the cellulose types employed. Section 9 describes the setup used for the experiments, whose results are reported in Section 10. Finally, Section 11 and Section 12 contain, respectively, considerations about sustainability aspects and validity, reliability, replicability and scalability of the work.

2 Essential theoretical background

Photocatalytic production of H_2 constitutes a way to use solar energy to obtain H_2 from water and, in case, a sacrificial agent. The process is enabled by a material, normally a semiconductor, that acts as a photocatalyst. This Section provides a theoretical background useful to understand the photocatalytic role of the semiconducting material, and how it allows to obtain H_2 from water and sunlight. The role of the sacrificial agent is also clarified.

2.1 The band theory of solid materials

The first step towards the understanding of the photocatalytic role of semiconducting materials, is recalling the band theory of solid materials. The band theory of solid materials relies on the assumption that, while in free atoms only discrete energy levels are possible for the electrons, corresponding to certain orbitals, in solid materials the energy levels of several orbitals overlap forming energy bands in which the energy of the electrons is allowed to change continuously. Two types of energy bands are formed: valence band (VB), in which the electrons are still bound to the atoms, and conduction band (CB), in which the electrons have enough energy to freely move within the solid phase. According to the distance in terms of energy that exists between VB and CB, a material can be classified as conductor, semiconductor or insulator. In conductors, VB and CB overlap, so that electrons are always allowed to move freely. In the case of semiconductors and insulators instead, between CB and VB there is a region in which no energy levels are available for the electrons. Electrons thus need to be excited by an external energy source to be able to jump into the CB and be free to move. The energy difference between the highest occupied molecular orbital (HOMO) of the VB, and the lowest unoccupied molecular orbital (LUMO) of the CB is the band gap of a material. An amount of energy equal or higher than the band gap has to be provided to excite an electron to the CB. Semiconductors are characterized by a relatively small band gap, while insulator have a much bigger band gap [10]. Figure 5 shows the energy bands of conductors, semiconductors and insulators.

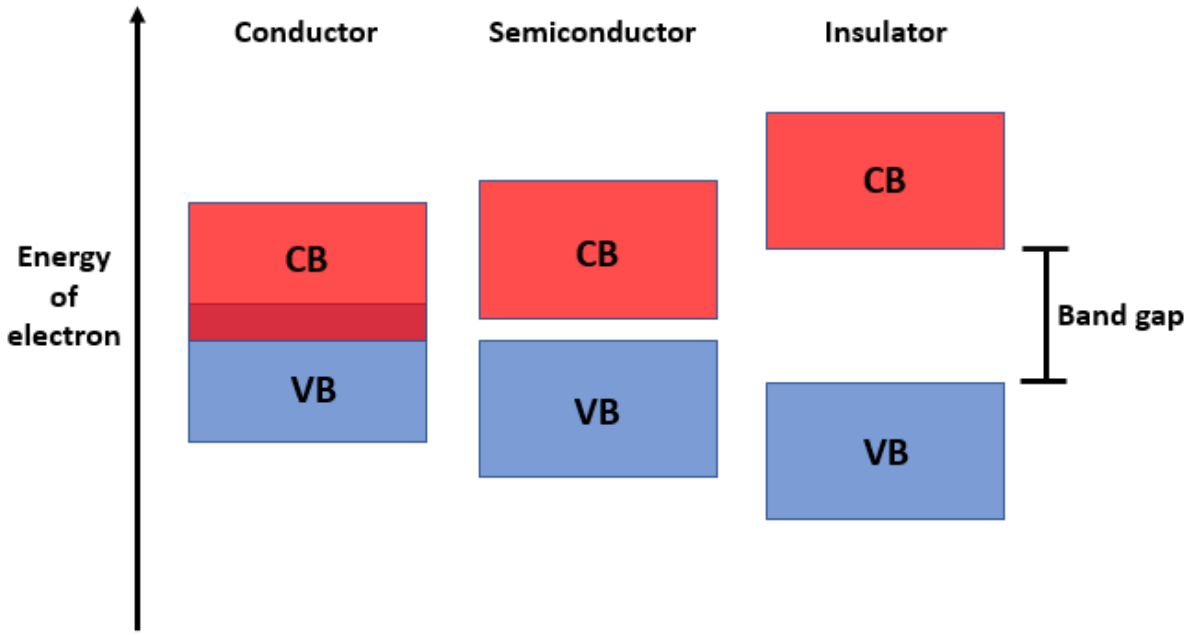

Figure 5: Schematic representation of VB and CB for conductors, semiconductors and insulators.

2.2 Photocatalytic water splitting and H_2 generation

According to the original idea, photocatalytic generation of H_2 is achieved by splitting H_2O molecules into H_2 and O_2 exploiting the properties of a semiconductor that acts as a photocatalyst.

As mentioned before, electrons in a semiconductor can be excited from the VB to the CB. This can be achieved when energy is supplied to the electrons by photons with energy higher than the band gap. Once an electron is excited to the CB, a vacancy is formed in the VB, resulting in the formation of so-called excitons or an electron-hole pair. According to the material considered, the photo-generated electrons and holes have certain electric potentials that can be expressed, for example, with reference to a Standard Hydrogen Electrode (SHE). If the potential of the holes is positive enough, they can oxidize water molecules according to two types of reactions shown hereunder [11]:

$$2H_2O \rightarrow O_2 + 4H^+ + 4e^-, \qquad E^0 = 1.23V \tag{1}$$

$$H_2O \rightarrow OH^\bullet + H^+ + e^-, \qquad E^0 = 2.73V \tag{2}$$

The reactions are reported together with the respective potential vs SHE at which they occur at pH 0, labeled as E^0. The potential of the holes should be at least higher than

this value for the corresponding reaction to occur. It is possible to notice that Reaction 1 requires a considerably lower potential than Reaction 2. Moreover, while Reaction 1 leads to the formation of O_2, Reaction 2 leads to formation of hydroxyl radicals $OH^{\bullet}$.

The electrons in the right side of both reactions are captured by holes generated in the VB of the photocatalyst, leaving protons in the reaction medium, while photoexcited electrons are used to reduce such protons according to the following reaction [12], resulting in evolution of H_2:

$$2H^+ + 2e^- \rightarrow H_2, \qquad E^0 = 0V \tag{3}$$

The reduction potential vs SHE is equal to 0 at pH 0 for the definition itself of SHE, and electrons must have a more negative potential for the reaction to occur.

The potentials needed for H_2O oxidation and H_2 evolution reactions are affected by the pH of the system. As Figure 6 shows, lower pH values are associated to potentials shifted towards more positive values and vice versa.

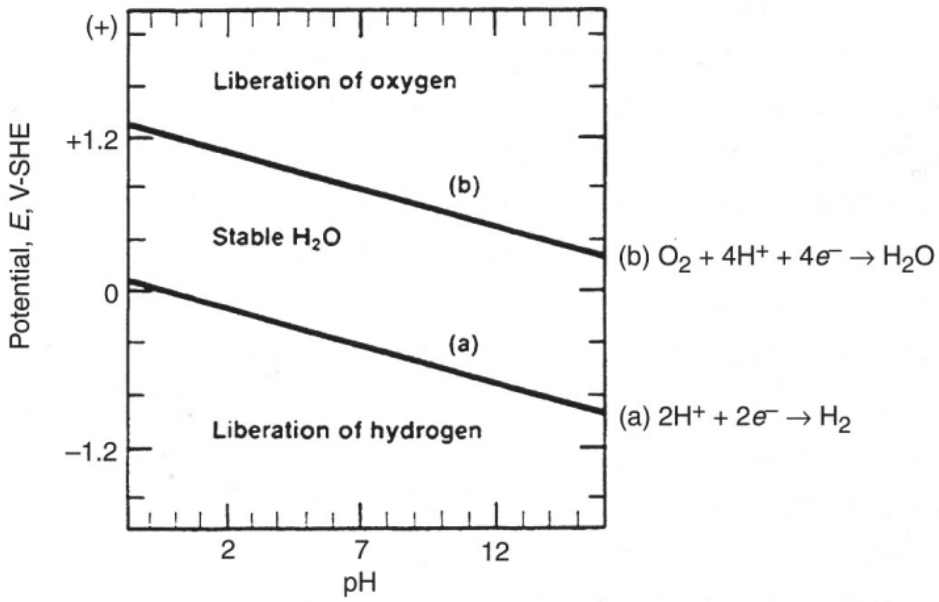

Figure 6: Influence of pH on O_2 evolution reaction and H_2 evolution reaction [13].

The semiconductor by itself does not participate directly in the reactions, but only acts like a catalyst and hence termed photocatalyst. Not every semiconductor is suitable for water splitting, since the mentioned constraints in terms of potential for holes and photoexcited electrons need to be satisfied to drive the process. As a reminder, at pH 0, the CB of the material should be able to host electrons at a voltage equal or lower than 0

V, while the holes generated in the CB should have a potential at least higher than 1.23 V for Reaction 1 and higher than 2.73 V for Reaction 2 to occur. A good indication of whether a semiconductor can be suitable or not is given by the position of its band gap. Figure 7 shows the band gap position of some common semiconductors.

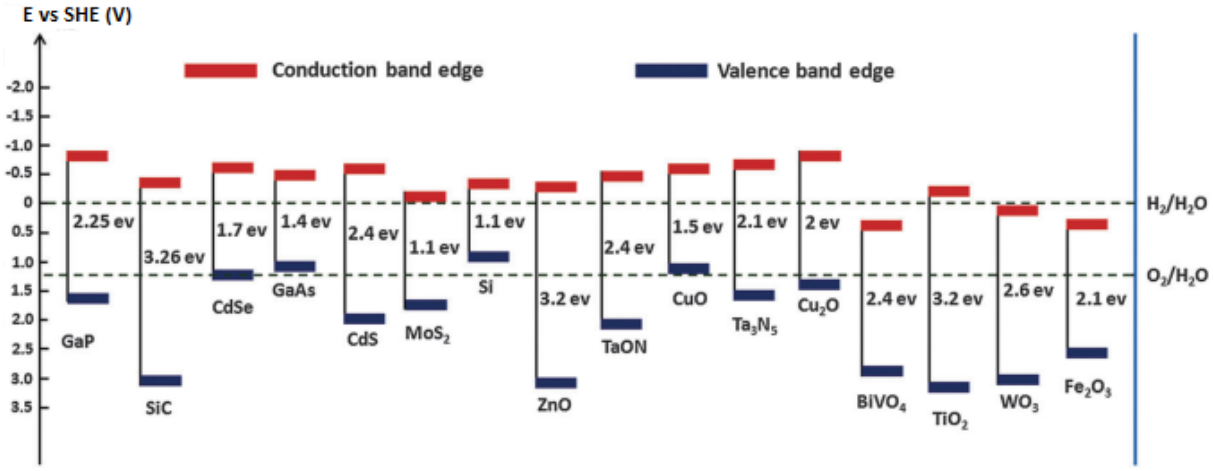

Figure 7: Band gap position of some common semiconductors [14].

Among the materials reported in Figure 7, titanium dioxide (TiO_2) is the most extensively studied, since the pioneering experiment of Fujishima and Honda in 1972, in which photocatalytic H_2 generation was shown for the first time using a titanium dioxide photo-anode in a photo-electrochemical cell (PEC) [15].

There are however important issues associated with the photocatalytic production of H_2 not yet discussed above. A major issue is the recombination of photo-generated charge carriers. Photo-excited electrons and holes, indeed, may not have the time to react in H_2O oxidation or protons reduction reactions, but can recombine resulting in a loss of efficiency for the photocatalytic process. Moreover, overpotentials are needed to drive the reactions. This means that, considering for example protons reduction according to Reaction 3, even if the theoretical voltage required is 0 V vs SHE at pH 0, a more negative potential is actually needed for the reaction to occur.

A common way to address both these issues is using a noble metal co-catalyst such as platinum (Pt), forming a junction with the photocatalyst. Pt can indeed act as an electron sink, capturing the photo-excited electrons and thereby reducing the probability of recombination, and reduce the over-potential needed for for the reduction of protons. Further information about possible strategies to improve the performances of the photocatalyst is provided in the literature review in Section 3.

As a final integration to this section, a schematic representation is shown in Figure 8

to summarize the water-splitting process. The figure shows a photocatalyst nanoparticle with a Pt nanoparticle as co-catalyst (top-right). Upon irradiation, a photon with energy higher than the photocatalyst's band gap is absorbed by the semiconductor and an electron is excited to the CB, leaving a hole in the VB. The hole is able to travel till the surface of the nanoparticle, where, according for example to Reaction 2, it can oxidize a water molecule generating a proton and a hydroxyl radical ($OH^{\bullet}$ radical), while the photo-excited electron is likely captured by the Pt co-catalyst and used for reduction of protons and H_2 evolution.

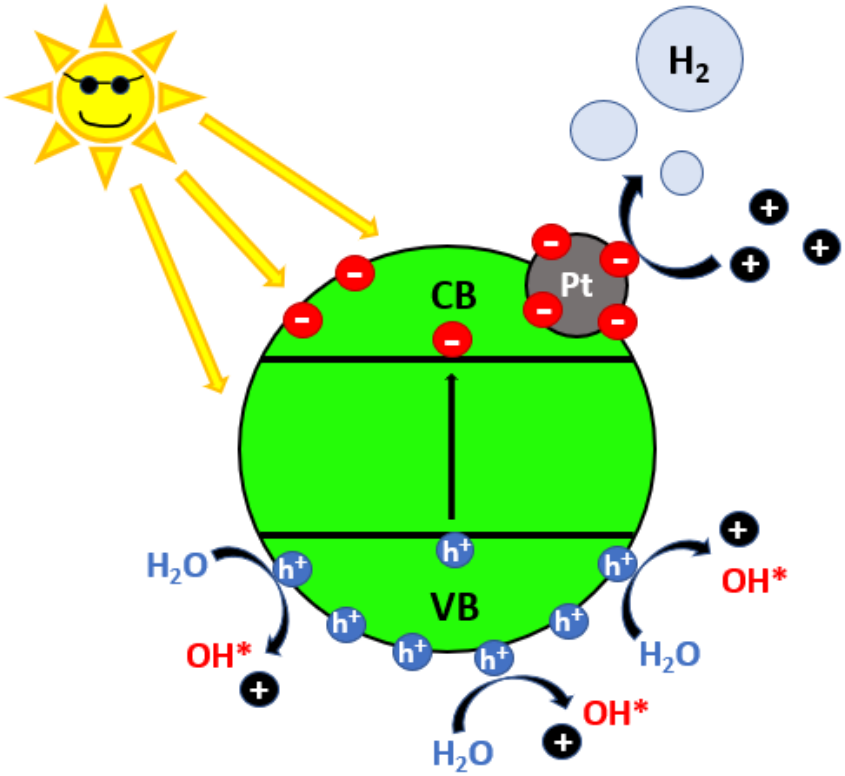

Figure 8: Schematic representation of water splitting process over a photocatalyst nanoparticle with Pt co-catalyst.

2.3 Beyond simple water splitting: introduction of sacrificial agents

In order to increase the efficiency of the photocatalytic process, sacrificial agents may be added to the system. Different types of sacrificial agents exist, but the way they work is similar. Good sacrificial agents are substances with a high reducibility. Examples are organic molecules such as methanol or glucose. Because of their high reducibility, sacrificial agents can be easily oxidized by photo-generated holes, providing electrons to the photocatalyst and thus acting as holes scavengers. This results in a reduction of the re-

combination rate of photo-generated charges, as every hole that reacted with a sacrificial agent's molecule is a hole that did not recombine with a photo-excited electron. Since sacrificial agents provide electrons to the photocatalyst, they are also known as "sacrificial electron donors" [16]. Though the principle is similar, every sacrificial agent is associated to a different particular set of chemical reactions. This section will clarify how cellulose works as a sacrificial agent, being this the main focus of the present work.

Cellulose is a polysaccharide that consists of linear chains of β-1,4 linked D-glucose units, usually insoluble in water. Its degree of polymerization ranges from several hundreds to more than ten thousands. A large quantity of hydroxyl groups is present along the cellulose chains, resulting in a well-ordered hydrogen bonding network and crystalline structure [9]. Figure 9 provides a graphical representation of the chemical structure of cellulose.

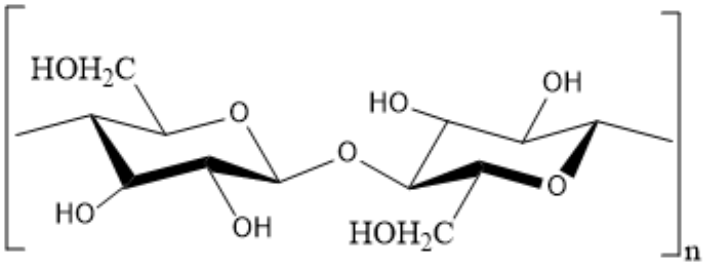

Figure 9: Chemical structure of cellulose.

When cellulose is used as sacrificial agent, it is first degraded to simpler and smaller molecules, which are in turn used for H_2 production. The first step of the degradation process is the cleavage of bonds between the glucose units, liberating glucose molecules in the system [12]. This can be achieved in the presence of protons and $OH^{\bullet}$ radicals, highly reactive species which have to be generated through simple water splitting as per reaction 2. The degradation reaction of cellulose to glucose is reported in Equation 4:

$$(C_6H_{10}O_5)_n + nOH^{\bullet} + nH^+ + ne^- \rightarrow n(C_6H_{12}O_6) \tag{4}$$

No H_2 molecule is generated at this stage and no hole has been scavenged, as the degradation of cellulose to glucose only requires the presence of species that have to be generated through simple water splitting. However, glucose and all the downstream products in the degradation chain can act as the hole scavengers mentioned above. Moreover, differently from cellulose, glucose and all the products of its degradation are soluble in water, enabling a much faster kinetics [12].

Once the structure of cellulose has been broken, glucose or smaller molecules are at first

adsorbed on the surface of the photocatalyst and are then readily oxidized by photo-generated holes and $OH^{\bullet}$ radicals, leading to the formation of H_2, CO_2 and CO as final products [12]. The set of intermediate reactions has not been exactly defined yet, but several different mechanisms have been proposed.

Chong et al. [17], for example, proposed a mechanism according to which glucose is at first degraded to arabinose, simultaneously producing formic acid (HCOOH) and H_2. Arabinose is then degraded to erythrose, and erythrose to glyceraldehyde, each step involving production of H_2 and formic acid. Formic acid can then be converted into H_2, CO_2 and, at a lower extent, CO. Figure 10 shows a graphical representation of the mechanism described.

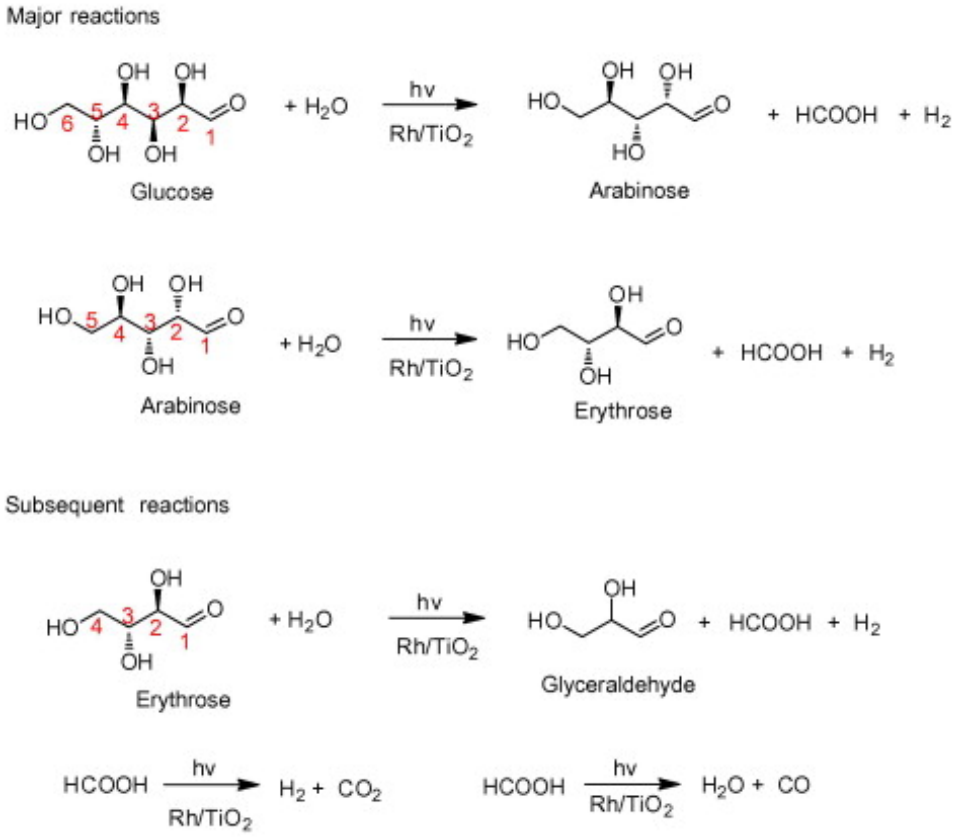

Figure 10: Possible mineralization pathways of glucose to H_2, CO_2 and CO [17].

Speltini et al. [18] instead proposed, as key intermediate in the degradation of glucose to H_2, the generation of hydroxymethylfurfural (HMF, $C_6H_6O_3$), which is the dehydrated product of glucose, able to efficiently react with the holes.

Several other studies ([19], [20]), despite proposing different sets of reactions, agree on a degradation path that includes continuous oxidation by photo-generated holes and pro-

duction of formic acid, H_2, CO_2 and CO.

Figure 11 finally shows a graphical representation of the phoyocatalytic H_2 generation process when cellulose is used as sacrificial agent, whose degradation products are able to react with photo-generated holes.

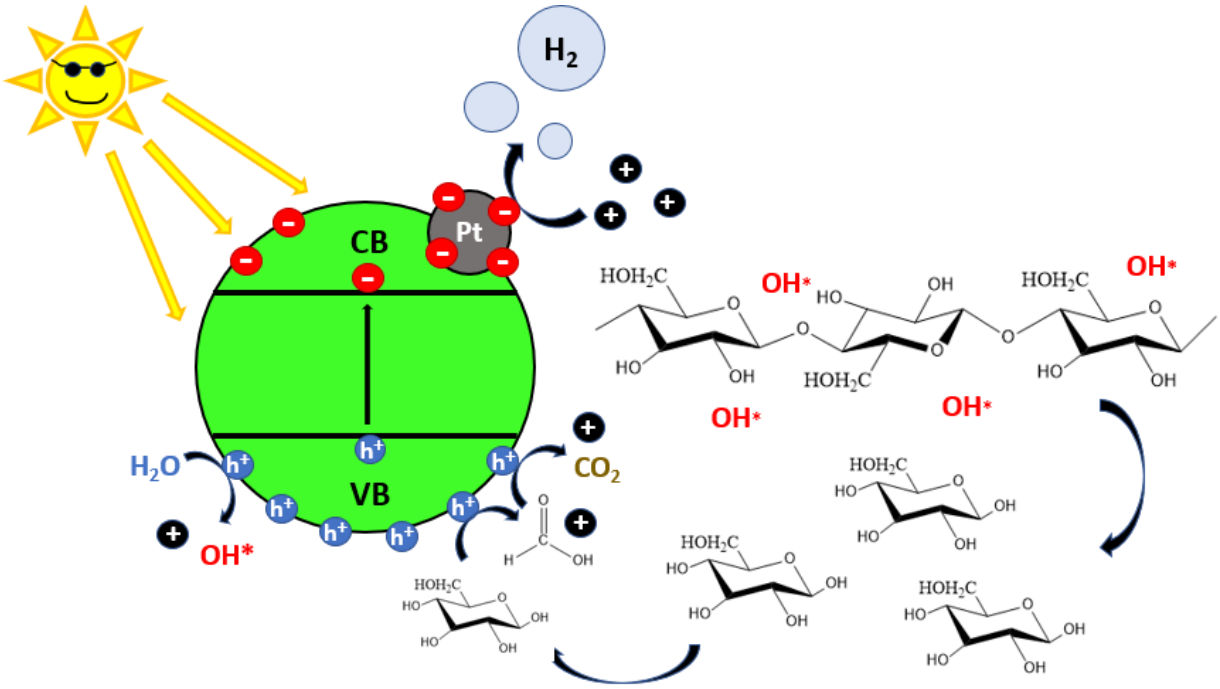

Figure 11: Photocatalytic generation of H_2 with cellulose as sacrificial agent. Cellulose is first broken into glucose units, which are in turn degraded by photo-generated holes with liberation of protons. Protons are reduced with evolution of H_2.

3 Literature review

This section aims at providing an overview of the past research about photocatalytic production of H_2. After a general introduction, the main strategies that over the years have been object of research to enhance the performances of such systems are summarized. Special attention will be given to studies in which cellulose is involved, as a particular case of the more general idea of introducing sacrificial agents to increase the efficiency of the system, that figures among the strategies mentioned.

The first study showing the possibility of photocataytic production of H_2 is the one conducted by Fujishima and Honda [15], in which a TiO_2-based photoanode was used in a PEC. Since that study, many attempts were done in order to improve the original idea.

Photocatalytic systems can generally be divided in 2 macro-categories: homogeneous and

heterogeneous systems. In homogeneous photocatalysis all the reacting species exist in the same phase, normally liquid. A homogeneous system typically involves an organometallic complex as catalyst and a photosensitizer [21]. In heterogeneous photocatalysis, instead, different phases can be identified, with a photocatalyst at the solid state opposed to a liquid phase [21]. Semiconducting materials are usually employed as photocatalysts for this type of application, exploiting the physical principles explained in Section 2.

Heterogeneous systems are the ones that have been most extensively studied, and can in turn be divided in other 2 sub-categories: PEC systems, as in Fujishima's and Honda's experiment [15], and systems where the photocatalyst is suspended in the form of powder in the reaction medium. Suspended systems showed advantages over PEC systems, such as higher simplicity and lower cost [22], as well as a higher surface area available per gram of photocatalyst, that boosts the chemical interactions. These characteristics led to the choice of a suspended system to carry out the present study.

Many semiconducting materials have been experimented as photocatalysts. Metal oxides with wide band gap, such as TiO_2 and zinc oxide (ZnO) are common examples. TiO_2 and ZnO have similar band gaps, around 3.2 eV, that corresponds to wavelength of 380 nm [23]. The main advantage of wide band gap materials is that they are suitable for both water oxidation and protons reduction, favoring the simplicity of the system. The other side of the coin is that they are only active under UV light, which accounts for a minor part of the solar spectrum. More recently, innovative materials such as graphitic carbon nitride (g-C_3N_4) appeared on the scene. g-C_3N_4 is characterized by a band gap significantly lower than that of TiO_2: 2.7 eV against 3.2 eV [23], theoretically allowing to absorb light up to 459 nm, but still keeping the ability to oxidize water and reduce protons in one single material [24]. Because of the smaller band gap, however, the water oxidation mechanism is the one reported in Equation 1, that does not involve generation of $OH^{\bullet}$ radicals but leads to O_2 evolution, making the material alone unsuitable for degradation of cellulose.

The achievement of an effective absorption of light is not the only necessity that characterizes a good photocatalytic system. Recombination of charges also severely affects the efficiency, as photo-generated holes and electrons may recombine instead of reacting with water and protons. In the attempt of overcoming one or both the issues mentioned, several strategies have been identified over the years:

- Deposition of noble metals nanoparticles (plasmonic photocatalysts);
- Synthesis of semiconductor-semiconductor heterojunctions;
- Engineered nanostructures;
- Doping;
- Dye sensitization;
- Introduction of sacrificial agents.

Deposition of noble metals nanoparticles such as Pt is helpful to reduce the recombination of charges, as the photo-excited electrons would be attracted and trapped by the noble metal particles. The light absorption in the visible spectrum would also be enhanced due to plasmon resonance, beside catalyzing the protons reduction reaction [12].

Semiconductor-semiconductor heterojunctions are useful to reduce the recombination and/or increase the absorption of visible light. Type 2 heterojunctions, i.e. heterojunctions with staggered band gaps, only help for reduction of recombination, while Z-scheme heterojunctions do both at the same time. An example of Type 2 heterojunction is the TiO_2/ZnO junction, explored in a several studies ([25], [26]) and schematically represented in Figure 12.

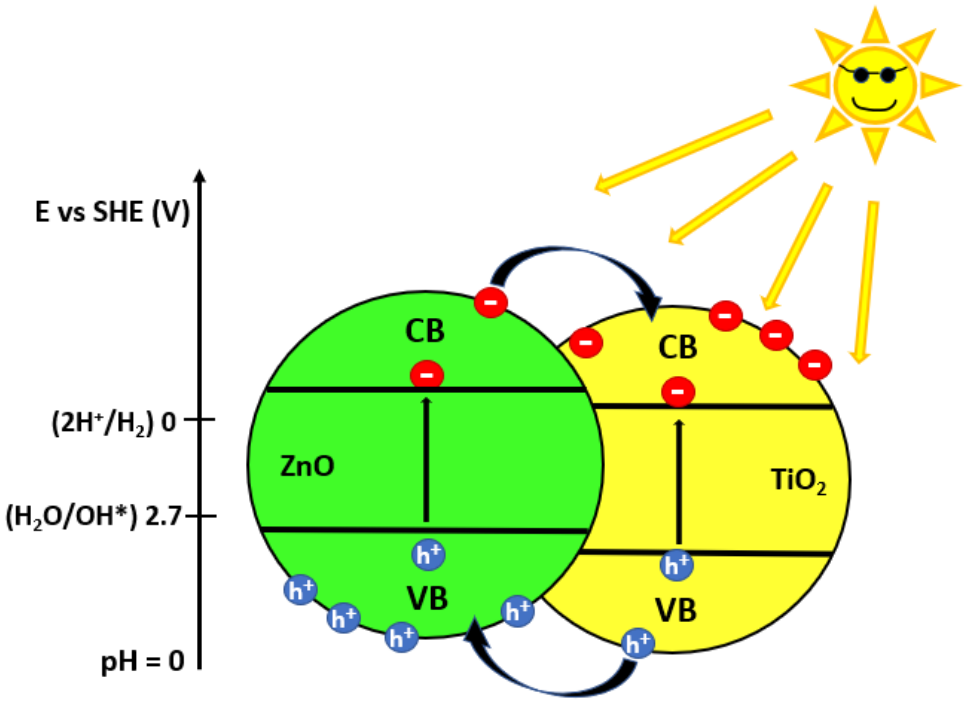

Figure 12: Schematic representation of TiO_2/ZnO heterojunction.

The staggered band gaps cause electrons to migrate to the CB with less negative potential, and holes to migrate to the VB with less positive potential. Consequently, the TiO_2 phase, having a less negative CB, will host most of the electrons, and ZnO phase, having a less positive VB, will host most of the holes. The result is an enhanced separation of charges and a reduced recombination, with TiO_2 being more active for reduction of protons and ZnO for oxidation of water. Other examples are the TiO_2/CdS and the Cu_2O/g-C_3N_4 junctions [23].

In Z-scheme junctions too, one material is active for water oxidation while the other

for H_2 evolution. Due to engineered favorable positioning of the band gaps and interface conditions, the excitation of electrons occurs in 2 steps: electrons are first excited from VB to CB of the material in charge of water oxidation and, after falling into the VB of the material in charge of H_2 evolution, they are excited to the CB of the latter material, where they can be used for reduction of protons. An example of Z-scheme investigated in literature is the WO_3/g-C_3N_4 junction ([23], [27]), for which a schematic representation is provided in Figure 13.

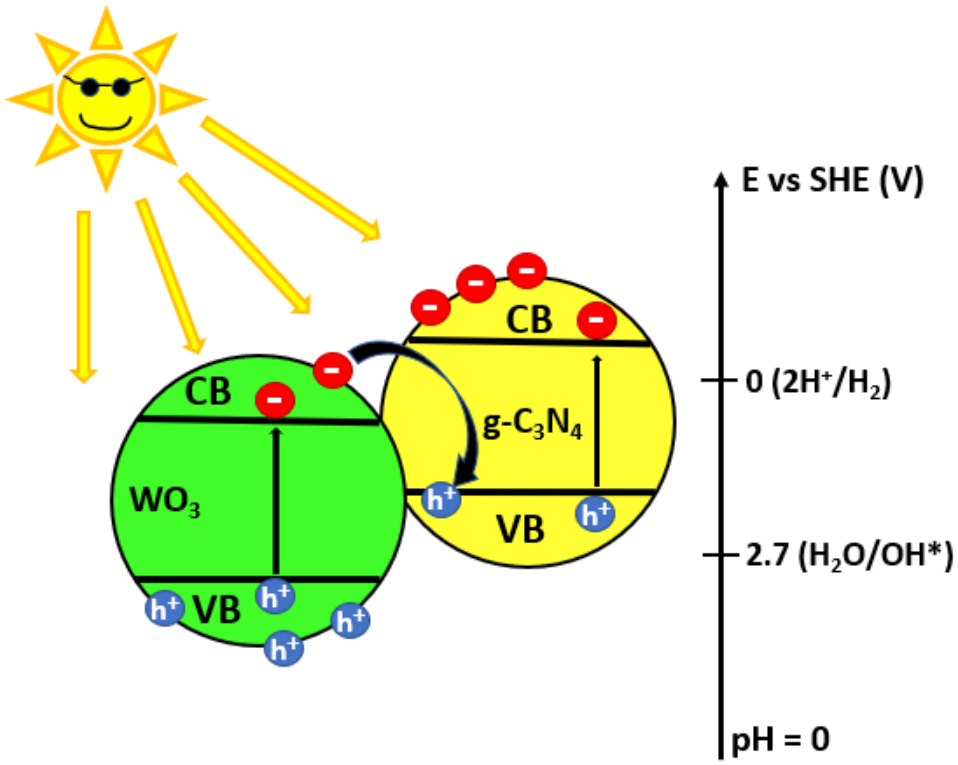

Figure 13: Schematic representation of WO_3/g-C_3N_4 Z-scheme.

Due to the 2-step excitation, it is possible to employ two materials with more narrow band gaps instead of one material with wider band gap, enabling the use of 2 less energetic photons instead of 1 more energetic photon and shifting the absorption towards longer wavelengths. Also in this case the separation of the charges is enhanced, as holes will stay in one material while electrons will migrate to the other. The Z-scheme is one of the most promising strategies to achieve a high efficiency. Further examples of Z-scheme are the TiO_2/g-C_3N_4, Nb_2O_5/g-C_3N_4 and Ag_3PO_4/g-C_3N_4 junctions ([23], [28]).

Doping a semiconductor by introducing impurities in its structure is another strategy to enhance the absorption of longer wavelengths. The impurities would introduce some intermediate states within the band gap of a semiconductor allowing, like for the Z-scheme,

an excitation in more than 1 step and red-shifting the absorption. Nonetheless, this strategy is not free of drawbacks: doping with metal impurities, for example, may lead to thermal instability that negatively affect the durability of the photocatalyst [29].

Dye sensitization, as the name suggests, aims at increasing the absorption of visible light by introducing a dye. Dyes are indeed able to absorb visible light, causing excitation of the electrons and injection into the CB of the photocatalyst, thus increasing the amount of electrons available for protons reduction. The electrons injected into the photocatalyst's CB should be replaced by electrons from a sacrificial agent [30]. Figure 14 schematically represents the concept.

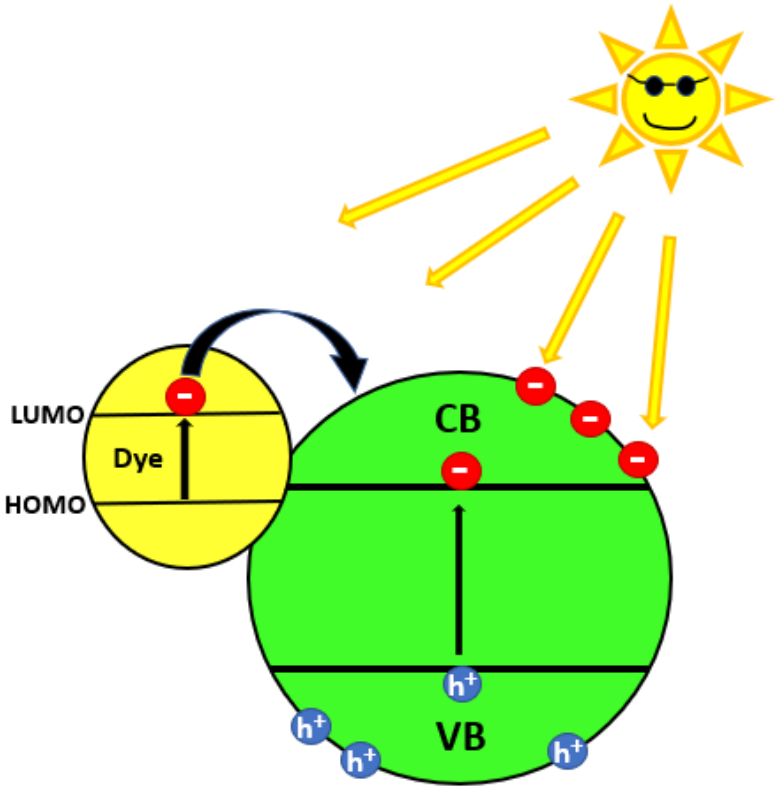

Figure 14: Schematic representation of dye sensitization mechanism.

A major drawback associated to the use of dyes is their self-degradation, that can cause instability and deactivation over time [30].

Introduction of sacrificial agents represents the last strategy to be mentioned, extremely important to ensure a good efficiency. Recalling what has been already explained in Subsection 2.3, their role is providing electrons to the photocatalyst compensating for the disadvantageous thermodynamics of the water oxidation reaction. Sacrificial agents

used in most studies are alcohols such as methanol and ethanol, due to the ease with which they can can be oxidized by photo-generated holes. However, alcohols are valuable and expensive fuels in industry, which would hinder their deployment in commercial applications [31]. Biomass derived substances and organic wastes such as triethanolamine, glycerol, glucose and cellulose have been proposed as cheaper, more suitable alternatives ([12], [31]). Being the most abundant organic polymer on earth [9] and, consequently, being characterized by high availability and low cost, cellulose represents a particularly interesting option as alternative sacrificial agent for photocatalytic production of H_2. Only limited number of studies have already been carried out about the topic, some of which are discussed here.

Caravaca et al. [12], for example, investigated the degradation of cellulose using TiO_2 as photocatalyst. Pt was used as co-catalyst for most of the experiments, even though other metals were also tested. The authors show that, when using commercial microcrystalline cellulose (Alfa Aesar) as sacrificial agent, the rate of production of H_2 dramatically improved with respect to a system without any sacrificial agent. The production follows a linear trend, which is kept till the end even in the longest experiments, whose duration was around 6 h. This suggests that steady state concentrations of molecules are reached and kept in the reactor. Glucose and fescue grass were also tested as sacrificial agents and the results compared with H_2 production in the presence of cellulose. As it could be expected, glucose, being the first product of the degradation chain of cellulose, shows a rate of production higher (approximately double) than that of cellulose at same concentration. Fescue grass, instead, being less refined and having a more complex structure, leads to a rate of production approximately half that of cellulose. Cellulose concentrations from 0.125 to 2 mg/mL were tested, obtaining a rate of production that increased with the concentration.

Speltini et al. [18] employed TiO_2/Pt as photocatalyst for the degradation of commercial fibrous long cellulose (Sigma Aldrich). Similarly to the research previously mentioned, different concentrations of cellulose were tested, showing that the production reduced when the concentration exceeded a certain value. An optimum was found around 6.7 mg/mL. An analogous study about the concentration of photocatalyst revealed an optimum at 2 mg/mL. However, it has not been investigated how the concentrations of cellulose and photocatalyst influence each other. Different pH values were tested, claiming best performances at the natural pH of the suspension, though without trying to justify why. Interestingly, the authors proposed an in-situ dye sensitisation mechanism enabled by HMF, reported to be a product of the degradation chain of cellulose. Rice husk was also tested as sacrificial agent, leading to a rate of production half of that of cellulose.

Chang et al. [32] also studied the influence of cellulose concentration, this time showing an optimum around 5 mg/mL, with TiO_2/Pt still being the photocatalyst. The different position of the optimum suggests that it is most likely dependent on factors such as concentration of photocatalyst and lighting conditions, usually different in each study. The

authors tried 2 types of cellulose with different crystallinity, and showed that a lower crystallinity enables better performances. The difference is attributed to the lower degree of polymerization, smaller particle size and higher water uptake when using less crystalline cellulose.

Wakerley et al. [33] used a CdS/CdO_x photocatalyst and showed a significant enhancement of the rate of production when KOH was added with a concentration of 10 M. In strongly basic conditions, indeed, cellulose becomes partially soluble in water, allowing a faster degradation. Moreover, different types of paper such as cardboard and newspaper, as well as biomass feedstocks like wooden branches, were successfully used as sacrificial agents in a solution of 10 M KOH.

Not much more is known about how different types of cellulose, or even cellulose derivatives, influence the rate of production, nor about the efficiency of conversion from light energy to H_2 energy of such a photocatalytic system. An estimate of the efficiency is essential to understand if the decrease of performances associated to the use of more rough feedstock, such as fescue grass, can be justified. The role played by parameters such as pH and mass concentrations is yet to be fully clarified, and an estimation of the concentration of $OH^\bullet$ radicals in the reaction medium is missing. Moreover, it is unknown how cellulose behaves compared to other sacrificial agents at similar conditions, and not much information is available regarding a photocatalyst tailored for this particular application, being most studies based on TiO_2.

4 Research questions and objectives

Considering what has already been achieved in literature and what is still unknown, the study will address the following research questions:

- What cellulose types/derivatives are most suitable to maximize the photocatalytic production of H_2?
- Is it possible to provide a better basic understanding of the process, clarifying how parameters such as pH and concentrations of cellulose and photocatalyst interact and affect the production?
- What is the concentration of $OH^\bullet$ radicals in the system?
- What conversion efficiency from light energy to H_2 energy is it possible to achieve?
- How does cellulose compare to other sacrificial agents?
- What kind of photocatalyst would be better suited for the application?

Through the research questions listed, the study aims at pursuing the following objectives:

- To validate the existing knowledge about photocatalytic degradation of cellulose for H_2 production, and further clarify its dynamics and key parameters;

- To assess how cellulose behaves in comparison to more common sacrificial agents;
- To develop a photocatalyst optimized for this particular application.

5 Scope and limitations

This research aims at assessing the potential of cellulose as sacrificial agent using a lab-scale experimental setup. The results obtained will only be valid, in numerical terms, for the particular conditions of the experiments. Different lighting conditions and different geometries of the reactor, for example, may indeed change the outcome, but this was not investigated. The objective of the study, however, is not trying to find optimal parameters valid in any configuration, but rather qualitatively describing the dynamics that characterize the system. The difference that the experimental conditions make hinders a comparison of the performances with those of the studies available in the literature. Costs-related dynamics were not taken into account.

6 Study design

In order to try to answer to the research questions mentioned above, the study has been structured as follows.

At first, a TiO_2/Pt photocatalyst was prepared as explained in Section 7. Several relevant types of cellulose were gathered (Section 8) and an experimental apparatus was set up (Section 9). After choosing an appropriate loading of Pt (Subsection 10.1), an estimation of the concentration of $OH^{\bullet}$ radicals in the system was performed (Subsection 10.2), and all the available types of cellulose were tested (Subsection 10.3). Using the type of cellulose that led to the best result, the influence of the concentrations of photocatalyst and cellulose was explored (Subsection 10.4), as well as the impact of pH (Subsection 10.5). The conversion efficiency from light energy to H_2 energy was then estimated (Subsection 10.6), taking into account all the information revealed by the previous experiments. The rate of H_2 production enabled by cellulose was compared to that enabled by other common sacrificial agents (Subsection 10.7) and, finally, some attempts were made to prepare a better performing photocatalyst (Subsection 10.8).

A flow chart of the steps followed during the research is provided in Figure 15.

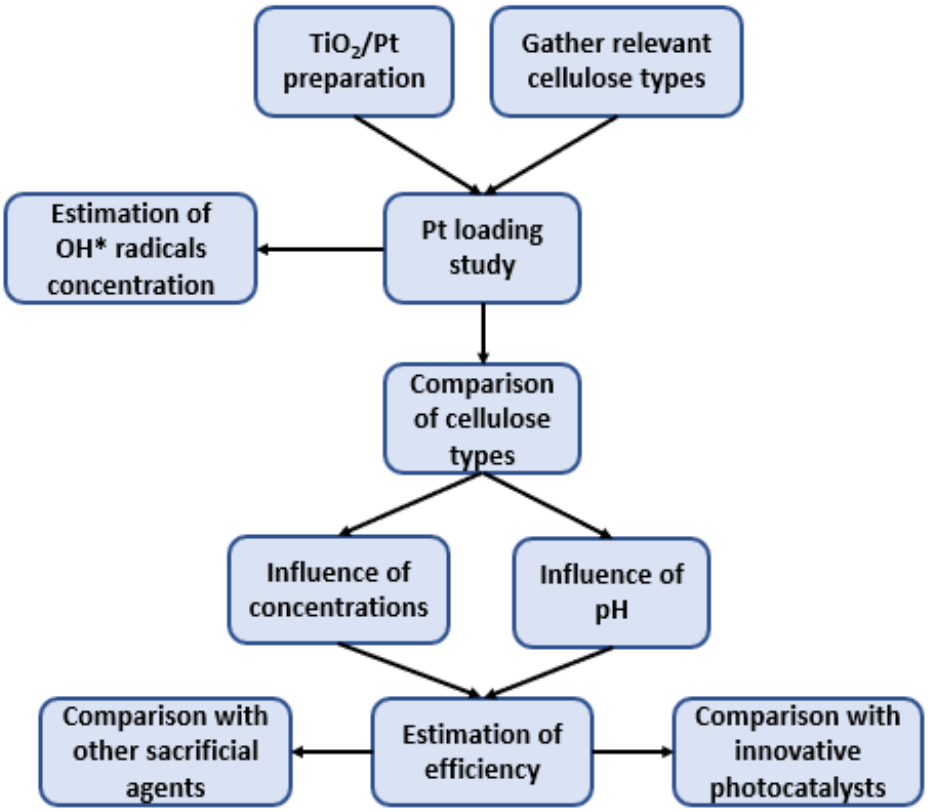

Figure 15: Flow chart of the steps followed during the research.

7 The photocatalyst

In order to initially focus the attention primarily on the the sacrificial agent side, TiO_2 was chosen as photocatalyst, whose dynamics and characteristics are well known and defined in the literature.

7.1 Material preparation

Commercial P25 TiO_2 (Sigma Aldrich, average particle size 25 nm) was employed and Pt nanoparticles were deposited in order to enhance the properties of the photocatalyst. Pt nanoparticles were obtained from a precursor, i.e., a 3 mM solution of H_2PtCl_6. A modified version of the procedure reported by Yao et al. [34] has been followed for Pt deposition.

Briefly, for a typical preparation, a certain amount of Pt precursor was diluted in deionized (DI) water reaching a total of 30 mL. 120 mg of sodium dodecylbenzenesulfonate (SDBS, Sigma Aldrich) were then dissolved, to obtain a SDBS concentration of 4 mg/mL. When the SDBS was completely dissolved, 150 mg of P25 were added. The amount of Pt

precursor used was such that the Pt mass introduced was equal to a chosen percentage of the mass of TiO_2. Three different Pt mass loadings on P25 were prepared: 0.2 %, 0.5 % and 1 %.
The suspension was ultrasonicated for 30 min and magnetically stirred for 1 h. It was then placed in an oil bath at 70 °C where it was kept under continuous stirring, and sodium borohydride ($NaBH_4$) was added as a reducing agent. The role of sodium borohydide was to reduce the Pt introduced with the precursor, so that it could nucleate and deposit onto the TiO_2 nanoparticles. The amount of reducing agent added was approximately 10 times the amount of Pt in terms of moles. The previously dissolved SDBS plays an important role: by behaving as a surfactant, it prevents agglomeration of particles and homogeneous Pt nucleation in the water, favoring heterogeneous nucleation onto TiO_2 nanoparticles. Also, the Pt layer on TiO_2 nanoparticles is reported to be thinner and better distributed when SDBS is added [34].
After adding the reducing agent, the suspension was aged for 2 hours in the oil bath and finally centrifuged to recover the particles. The latter were rinsed, dried overnight at 60 °C and stored for future use. Generally, higher the Pt loading, darker was the appearance of the powder, suggesting an increase of visible light absorption caused by Pt deposition.

7.2 Material characterization

In order to compare the light absorption properties of the prepared material to those of commercial P25, UV-vis spectroscopy was used. Suspensions of 1 mg of P25 in 6 mL DI water, and 1 mg of as prepared photocatalyst with 0.5 % Pt loading in a same amount of DI water were compared in the range 300-800 nm. The results are shown in Figure 16.

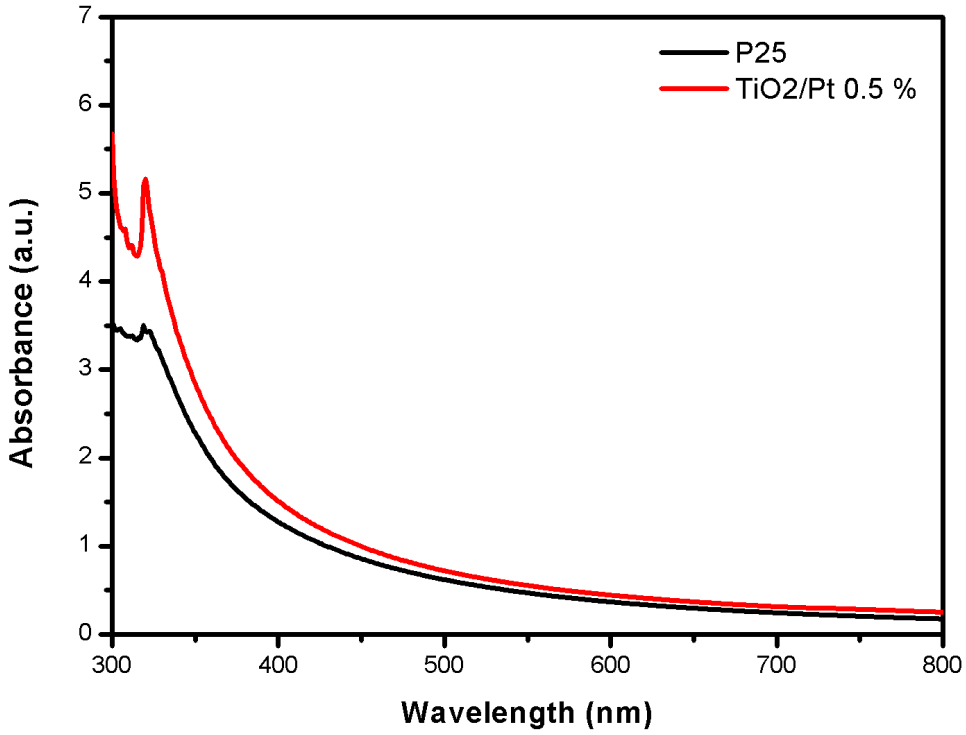

Figure 16: Light absorbance of P25 and prepared TiO_2/Pt 0.5 %

The figure shows, in both cases, a weak absorption in the visible range that quickly increases below 400 nm, consequently to the large band gap of the material. An enhancement of the light absorption at all wavelengths is observed after Pt deposition.

Photoluminescence spectroscopy (PL spectroscopy) was used to verify that the recombination of photo-generated charges is actually reduced after deposition of Pt. PL spectroscopy consists in measuring the intensity of the fluorescent light emission of a sample in a certain wavelength range, during its excitation at a fixed wavelength. The analysis relies on the fact that the recombination of holes and electrons within a photocatalyst is associated to emission of photons. The excitation of a photocatalyst sample at a wavelength able to excite its electrons should thus cause fluorescent emission of photons as a consequence of the recombination, whose intensity can be observed and measured. The deposition of Pt, by reducing the recombination, is expected to decrease the intensity of the fluorescent emission [23]. Thus, 2 samples of P25 and TiO_2/Pt 0.5 % with same concentration of 1 mg in 320 mL were prepared. When excited at 375 nm, the samples showed an emission peak around 760 nm, whose amplitude decreased of about 4 times when passing from P25 to TiO_2/Pt 0.5 %. This result represents a confirmation of the reduction of recombination

caused by Pt deposition.

8 Cellulose types studied

In order to try to maximize the performances in terms of H_2 production, and to broaden the understanding about cellulose degradation, several types of cellulose were tested as sacrificial agent. Most of the samples tested were natural types of cellulose provided by the Department of Fibre and Polymer Technology, KTH Royal Institute of Technology and are reported in Table 1, which also contains information about molecular structure and crystallinity index.

Table 1: Cellulose types provided by Department of Fibre and Polymer Technology, KTH

Cellulose type	Molecular structure	Crystallinity index
Rapeseed cellulose	Cellulose 80 % Hemicelluloses 11 % Lignin 8 %	not available
H_2O_2 bleached rapeseed cellulose	Cellulose 85 % Hemicelluloses 8 % Lignin 6 %	83 %
Cellulose nanofiber from spruce pulp	Cellulose 99 %	79 %
U. fenestrata algae cellulose	Cellulose 85 % Xyloglucan 15 %	48 %
Regenerated U. fenestrata algae cellulose	Cellulose 90 % Xyloglucan 10 %	63 %

The crystallinity index is a measure of how strong are the interactions among cellulose chains due to hydrogen bonds. Cellulose types with lower crystallinity indices, such as cellulose from U. fenestrata algae, are expected to be easier to degrade and to enable higher rates of H_2 production. Regenerated U. fenestrata algae cellulose was obtained by purification of U. fenestrata algae cellulose followed by dissolution and precipitation. The crystallinity index increased slightly, but the sample was much finer and easier to disperse. Cellulose types that contain lignin (like rapeseed cellulose, both bleached and non-bleached), are instead expected to be harder to break down, being lignin a structural material in the tissues of plants that provides rigidity and resistance to degradation [35]. In addition to the mentioned cellulose types, two commercial cellulose derivatives have been considered in this study: carboxymethyl cellulose (CM cellulose, Merck) and sodium carboxymethyl cellulose (Na CM cellulose, Carl Roth). CM cellulose is a derivative of common cellulose in which some hydroxyl groups are substituted with carboxymethyl groups (-CH_2-COOH) [36]. Because of the polar carboxyl group COOH, this kind of

cellulose is reported to be soluble in water [36], that was considered to be beneficial for faster kinetics of chemical reactions. Figure 17 shows a representation of the chemical structure of the fundamental unit of CM cellulose.

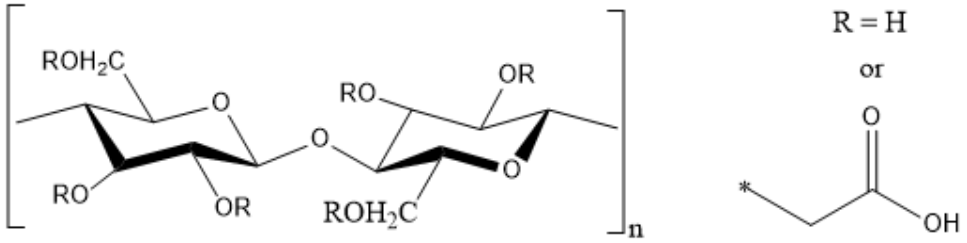

Figure 17: Chemical structure of CM cellulose

Na CM cellulose is similar to CM cellulose, but sodium carboxymethyl groups CH_2COONa are introduced instead of CH_2COOH groups, as shown in Figure 18. For this reason, this cellulose type exists in the form of salt.

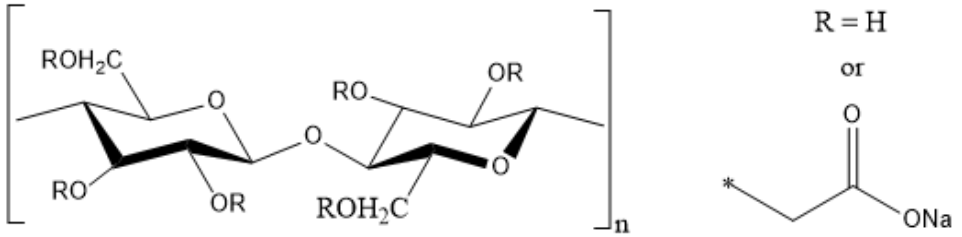

Figure 18: Chemical structure of Na CM cellulose.

As a result of this structure, when immersed in water, molecules dissociate in anions and Na^+ cations, leading to an enhanced solubility.
The properties of both CM cellulose and Na CM cellulose, water solubility in particular, depend on their degree of substitution (DS), i.e, the number of hydroxyl groups which are substituted by carboxymethyl groups, on average, in a fundamental unit. Higher the DS, in general, higher the solubility [37]. Actually, during the experiments, it was not possible to achieve the complete dissolution of CM cellulose and Na CM cellulose. The particles were however much smaller than the other types of cellulose, better dispersed and the suspension as a whole much more transparent.

Because of the good results obtained with Na CM cellulose, the KTH Department of Fibre and Polymer Technology provided another type of charged cellulose: TEMPO-oxidized cellulose. Oxidation by TEMPO is an alternative, recent and energy-efficient method to introduce COONa groups in the structure of natural cellulose [38]. The goal, like for Na CM cellulose, is to achieve solubility through dissociation into anions and Na^+ cations.

In this case however, instead of CH_2COONa groups, more simple COONa groups are introduced. Figure 19 shows the chemical structure of TEMPO-oxidized cellulose.

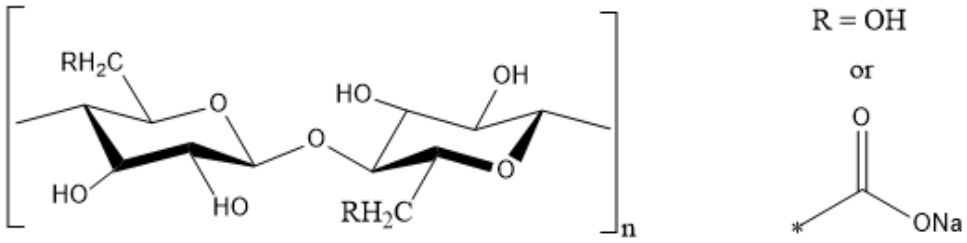

Figure 19: Chemical structure of TEMPO-oxidized cellulose.

9 Experimental setup

The experiments were run in a 3 necks round-bottomed pyrex glass flask with rated capacity 25 mL, filled with 25 mL of suspension of water, photocatalyst and cellulose. The suspension was magnetically stirred at 500 rpm during the experiments.

The light source used was a OSRAM Ultra-Vitalux 300 W lamp, that simulates natural sunlight. The spectral radiation distribution of the lamp provided by the manufacturer is reported in Figure 20.

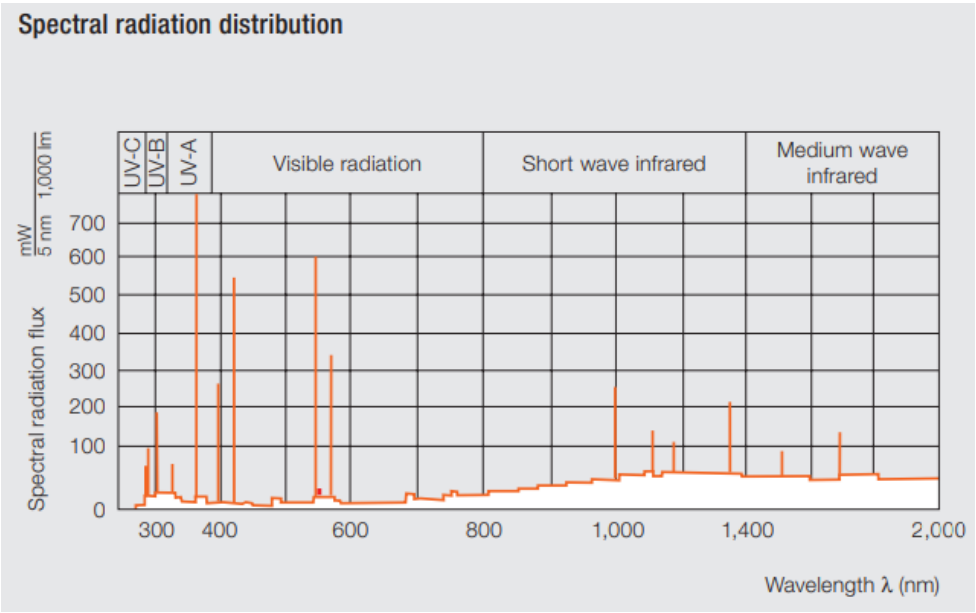

Figure 20: Spectral radiation distribution of OSRAM Ultra-Vitalux lamp [40].

It is possible to appreciate, like for natural sunlight, emission in the UV region, i.e. at

wavelengths lower than 400 nm. The UV-A and UV-B emitted radiations account for, respectively, 13.6 and 3 W according to the manufacturer [40]. The UV emission thus constitutes 5.5 % of the total emission, value similar to that occurring for solar radiation falling on earth, around 6 % [41]. In the case of natural sunlight however, as it can be observed in Figure 21, the emission is generally shifted towards shorter wavelengths, with peak emission occurring in the visible range. The peak emissions of the lamp used occurs instead in the IR region.

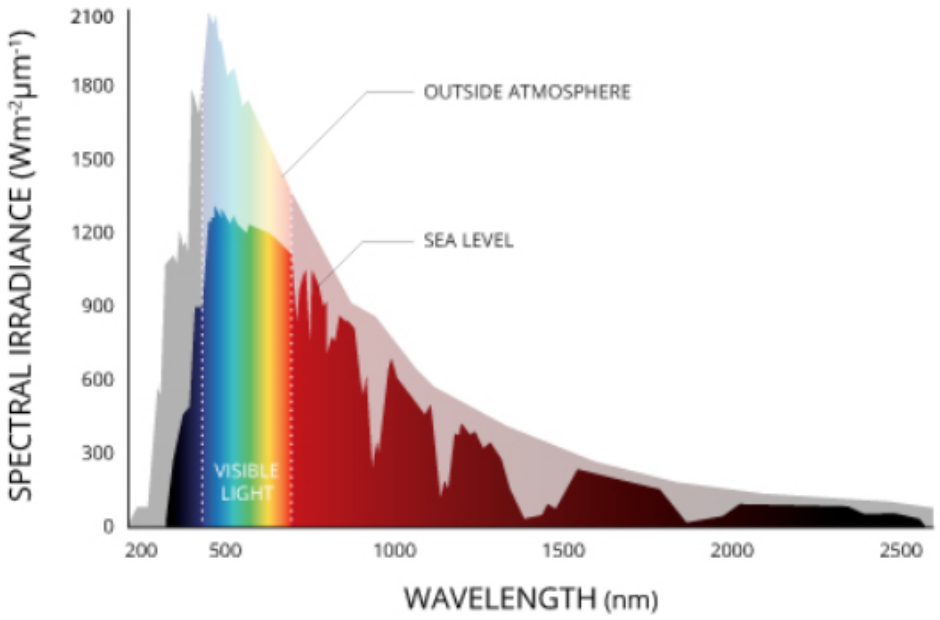

Figure 21: Spectral radiation distribution of natural sunlight [42].

That lamp was placed at a distance such that the irradiation flux on the sample was around 1000 W/m^2.

Temperature and concentration of H_2 were sensed in the gas phase of the sealed reactor with Unisense sensors, able to give in real time the H_2 concentration in μmol/L and the temperature in °C. The working principle of the sensor and the details about the calibration are reported in Appendix 1. A fan was used to keep the temperature stable. The reactor was sealed with rubber caps, and the sensors were introduced inside the system by using their tips to penetrate the rubber. A grease was then added in proximity of the holes to ensure that no leakage occurred. Figure 22 shows a picture of the experimental setup.

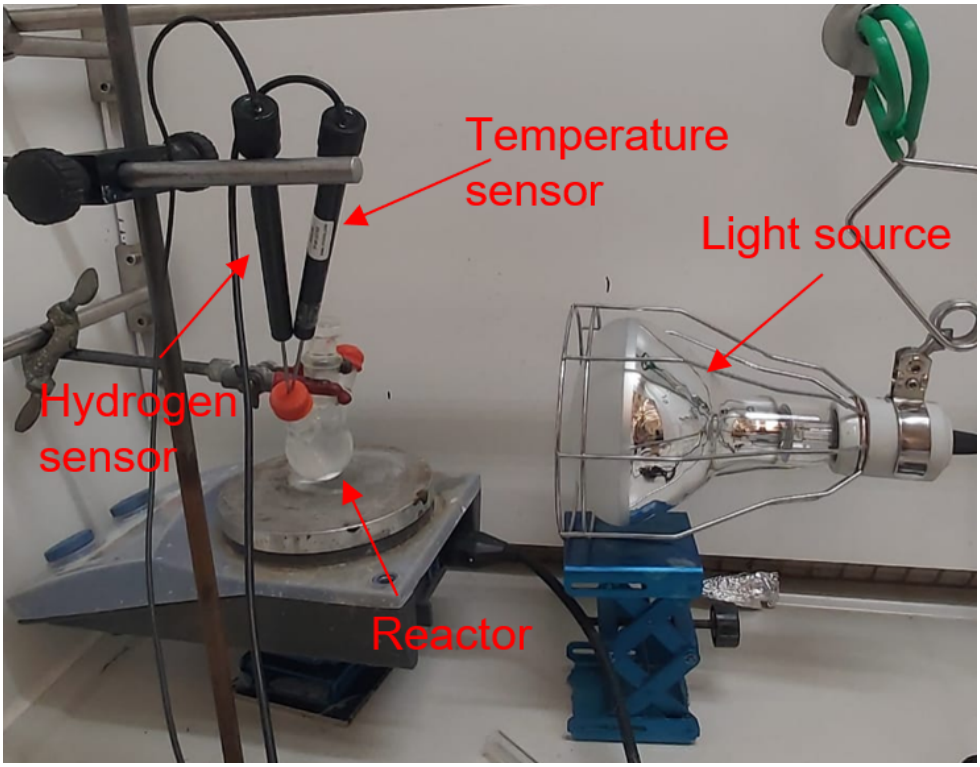

Figure 22: Experimental setup.

10 Results and Discussion

This section summarizes the results obtained from the experiments. At first, it is useful to consider the outcome of a typical experiment. Figure 23 shows the variation of the H_2 concentration sensed in the gas phase of the reactor, with reference to a typical experiment performed with TiO_2/Pt 0.5 % with a concentration of 0.3 mg/mL, and a concentration of regenerated U. fenestrata algae cellulose of 0.25 mg/mL.

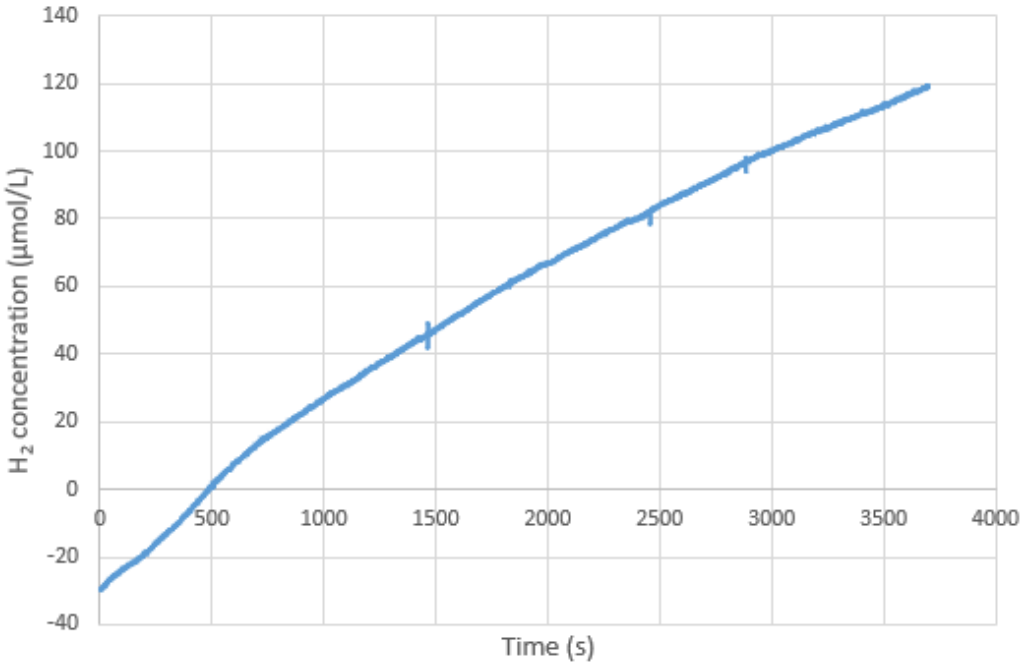

Figure 23: Evolution of H_2 concentration in a typical experiment carried out with 0.3 mg/mL of TiO_2/Pt 0.5 %, and 0.25 mg/mL concentration of U. fenestrata algae cellulose.

Coherently with the results previously obtained in the literature, the variation of H_2 concentration follows a linear trend. The irregular initial part is due to the temperature transition from ambient temperature to the steady state temperature of the experiment, and to the time needed to saturate the suspension with H_2. The rate of H_2 generation in μmol/h has been chosen as the key indicator to compare different experiments, and it can be obtained as follows. After exporting the results in excel, a linear interpolation of the concentration evolution in the steady state part of the experiment can be used to know the slope of the line and thus the rate of change of the concentration in μmol/L/s. By multiplying such value with the volume of the gas phase, measured as the difference between the total capacity of the reactor and the volume of the suspension, it is possible to obtain the rate of H_2 production in μmol/s, subsequently converted in μmol/h.

10.1 Influence of Pt loading

As a first step of the experiments, a study was conducted to assess the influence of Pt loading on the H_2 production. Four different mass percentages have been tested, namely 0

%, corresponding to pure P25, 0.2 %, 0.5 % and 1 %. The experiments have been conducted with a photocatalyst concentration of 0.3 mg/mL and a CM cellulose concentration of 1 mg/mL. The results are plotted in Figure 24.

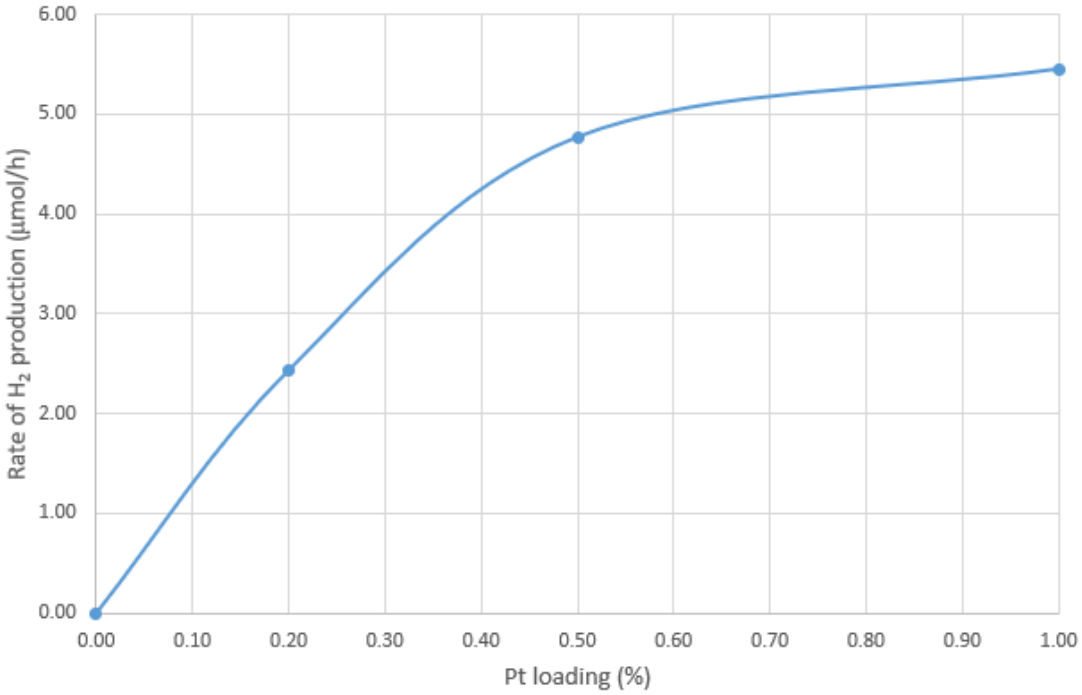

Figure 24: Influence of Pt loading on H_2 production.

Figure 24 shows a negligible production when no Pt is used, and a conspicuous improvement when a mass ratio of Pt as low as 0.2 % is used. A further considerable increase in the rate of H_2 production was observed in the presence of 0.5 % Pt, while with 1 % Pt, despite doubling the noble metal amount, only a marginal improvement was noticed.

The results are in agreement with previous studies [12]. On the one hand, increasing the Pt content the recombination of photo-generated charge carriers is reduced, and the reduction of protons becomes more simple due to a higher number of active sites available, where the reduction can happen at a low overpotential. On the other hand higher Pt contents may lead to agglomeration of Pt nanoparticles and excessive shading of TiO_2 nanoparticles from the light source, counterbalancing the beneficial properties provided.

Given the results found, a Pt mass percentage of 0.5 % was chosen as the optimum and used for all the following experiments.

10.2 Estimation of concentration of $OH^{\bullet}$ radicals

Prior to any further experiment about H_2 production, an estimation of the concentration of $OH^{\bullet}$ radicals in a photocatalytic system containing TiO_2/Pt 0.5 % was performed, using terephthalate (TPA) as a probe. TPA readily reacts with photo-generated $OH^{\bullet}$ radicals forming, among the possible reaction products, hydroxyterephthalate (hTPA) [43] as in Figure 25:

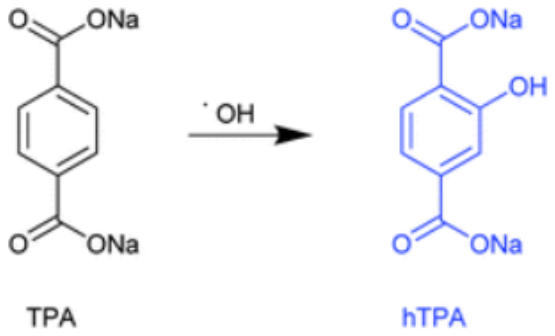

Figure 25: Reaction of TPA with $OH^{\bullet}$ radicals to form hTPA [43].

hTPA is a fluorescent molecule whose presence can be detected using photoluminescence (PL) spectroscopy. It is indeed stated in literature that, when excited at a wavelength of 325 nm, hTPA shows a peak fluorescent emission at 425 nm [43]. A higher concentration of hTPA will be associated to a stronger fluorescent emission at 425 nm. A calibration in which several known concentrations of hTPA are associated to the corresponding intensity of the emission peak at 425 nm, allows then to find the unknown concentration of hTPA in a sample knowing the intensity of the fluorescent emission at 425 nm. Details about the calibration are reported in the Appendix 2.

Once the concentration of hTPA is known, it is possible to find the steady state concentration of $OH^{\bullet}$ radicals in the system from the kinetic equation of the formation reaction of hTPA from TPA [43]:

$$\frac{d[hTPA]}{dt} = k[TPA][OH^{\bullet}]_{ss}Y \tag{5}$$

where k is the rate constant of the reaction and Y represents the fraction of TPA molecules reacted with $OH^{\bullet}$ radicals that form hTPA. Their values are reported to be, respectively, $4.4{\cdot}10^9$ $M^{-1}s^{-1}$ and 0. [43].
In this case, 25 mL of a 500 μM TPA solution were used for the experiment. TiO_2/Pt 0.5 % was suspended at a concentration of 0.3 mg/mL and the sample was irradiated for 5 min. After centrifugation to remove the photocatalyst powder, the sample was analyzed

with PL spectroscopy, and a concentration of $OH^{\bullet}$ radicals around $5.5 \cdot 10^{-15}$ M has been estimated. More details about the calculations are provided in Appendix 2.

10.3 Comparison of different types of cellulose

All the types of cellulose mentioned in Section 8 have been tested for H_2 production, and the results are reported in the current section. In order to perform a fair comparison, the same conditions have been set for all the experiments: a cellulose concentration of 0.25 mg/mL and a photocatalyst concentration of 0.3 mg/mL, while the initial pH was adjusted to 6 using HCl and NaOH. Cellulose was dispersed by ultrasonication of the sample. For comparison, an experiment without cellulose has also been performed, in which H_2 is obtained from pure water splitting. The results are reported in Figure 26.

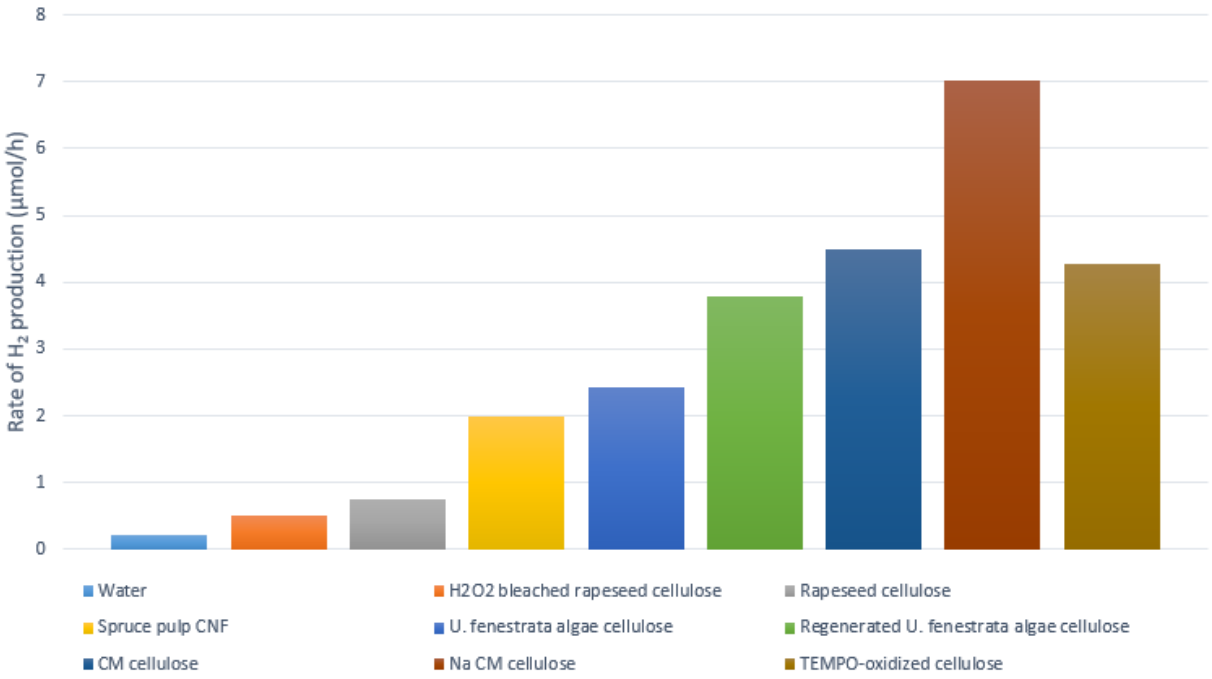

Figure 26: Rate of H_2 production from water and different cellulose types.

The figure shows a very modest production for pure water splitting and a considerable improvement when cellulose is introduced into the system, the magnitude of the improvement depending on the type of cellulose. This confirms the primary role played by the sacrificial agent in the photocatalytic reaction.

Among the natural types of cellulose, it is possible to note how those having a smaller crystallinity index (U. fenestrata algae cellulose and Regenerated U. fenestrata algae cellulose) led to the highest rates of production of H_2. As mentioned earlier, indeed, a lower

crystallinity index is associated to weaker chemical bonds, that implies easier degradation. Moreover, the water-soluble xyloglucan contained in U. fenestrata algae cellulose and Regenerated U. fenestrata algae cellulose may also contribute to the good performances observed. Rapeseed cellulose types led instead to much slower production rates. As a consequence of their chemical composition (high crystallinity index and presence of lignin), not only those types of cellulose are more difficult to chemically degrade, but also to physically break and disperse, resulting in bigger particles. Bigger particles in turn translated into high instability of the suspension and fast agglomeration of particles, with both cellulose and TiO_2 precipitating and negatively affecting the corresponding production rates. A similar tendency has been observed, though at a smaller extent, with spruce pulp CNF, which is also characterized by a high crystallinity index.

It was in the attempt to overcome the issue of agglomeration that cellulose concentration and initial pH were chosen.
In order to reduce the tendency to agglomeration, a relatively small concentration of cellulose (0.25 mg/mL) was used, while studies in the literature ([12], [18]), that employed commercial cellulose, used concentrations of several mg/mL.
The understanding of the choice of the initial pH, requires the introduction of the concept of zeta potential, which is strongly related to the stability of a suspension. The zeta potential is a measure of the net electric charge on the surface of the particles of a suspension. The more the zeta potential of a suspension with one type of particles is far from 0, the more the suspension tends to be stable, due to the repulsive Coulombian forces among particles [44]. The net charge on the surface of the particles is dependent on the pH of the suspension. Generally, higher pH values are associated to more negative values of zeta potential, while the opposite is true for lower pH values.
The photocatalytic system here considered is a suspension of two types of particles: P25 TiO_2 with Pt nanoparticles and cellulose. The zeta potential of P25 as a function of the pH is available in the literature and shown in Figure 27. The deposition of Pt is reported not to significantly affect the zeta potential [45].

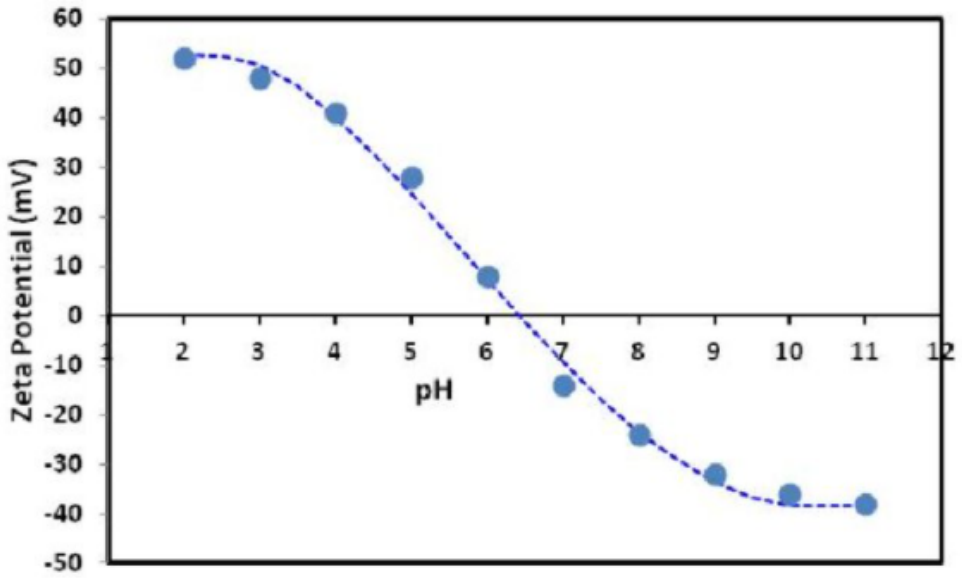

Figure 27: Zeta potential curve of P25 TiO_2 [46].

Figure 27 shows that the point where the net charge is 0, called isoelectric point, falls between pH 6 and 7, meaning that the pH must be far enough from that point for the TiO_2 suspension to be stable. It is now necessary to anticipate a result which is better clarified in Subsection 10.5: whenever the initial pH was adjusted to a value higher than 5, the pH measured at the end of the experiment was equal to 5. This means that, if the initial pH is adjusted to a value above the isoelectric point of P25, between 6 and 7, the suspension would cross it on its way to pH 5, causing instability. As a consequence, the zeta potential of P25 imposes a first constraint on the initial pH: it is not desirable to start from a pH higher than that corresponding to the isoelectric point of P25.

On the other hand, being part of the suspension, cellulose must also be taken into account. H_2O_2 bleached rapeseed cellulose has been considered as an example, and its zeta potential at various pH has been measured and shown in Figure 28.

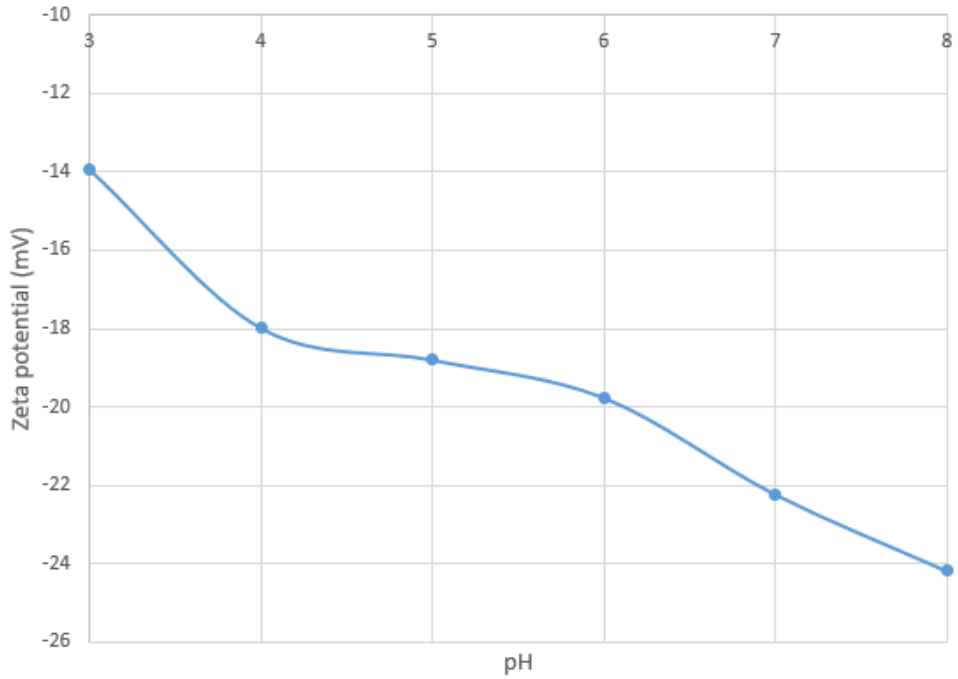

Figure 28: Zeta potential curve of H_2O_2 bleached cellulose

The figure displays a negative zeta potential for all the pH studied, most probably as a consequence of the negatively charged OH groups abundant in the structure of any kind of cellulose. This means that for pH values lower than 6, P25 and cellulose have zeta potential of opposite signs, and the lower the pH, higher the difference between the potentials tends to be. As an implication, at pH 5, which is the pH reached by the system starting from any higher pH, as well as at any lower pH, there will be an attraction among TiO_2 and cellulose particles that may cause the agglomeration observed experimentally. This mechanism can explain the agglomeration observed, and justifies the choice of an initial pH just below the isoelectric point of P25.

This strategy worked for spruce pulp CNF, but not for rapeseed cellulose types, that eventually agglomerated anyway. No agglomeration issues were observed with other types of cellulose, being easier to obtain a well dispersed suspension.

These considerations might explain the behavior previously observed in the research carried out by Speltini et al. [18], in which the best performances were obtained at the natural pH of the suspension, which is close to 6 for DI water slightly acidified by CO_2.

Finally, it is worth noting the good rates of production enabled by CM cellulose, Na CM cellulose and TEMPO-oxidized cellulose, with Na CM cellulose leading to the best result. This comes as a consequence of the introduction of, respectively, CH_2COOH, CH_2COONa and $COONa$ groups that successfully enhance the dispersibility and reduce

the effort needed for chemical degradation. Since Na CM cellulose gave the best results, all the following experiments mostly focus on this type of cellulose.

10.4 Influence of cellulose and photocatalyst concentration

An analysis aiming at studying the influence of cellulose and photocatalyst concentration is here reported.

At first, experiments were conducted keeping constant the concentration of photocatalyst to the value of 0.3 mg/mL used so far, and varying the concentration of cellulose between 0.25 and 5 mg/mL. The experiments have been done for CM cellulose and Na CM cellulose, and the results are reported in Figure 29.

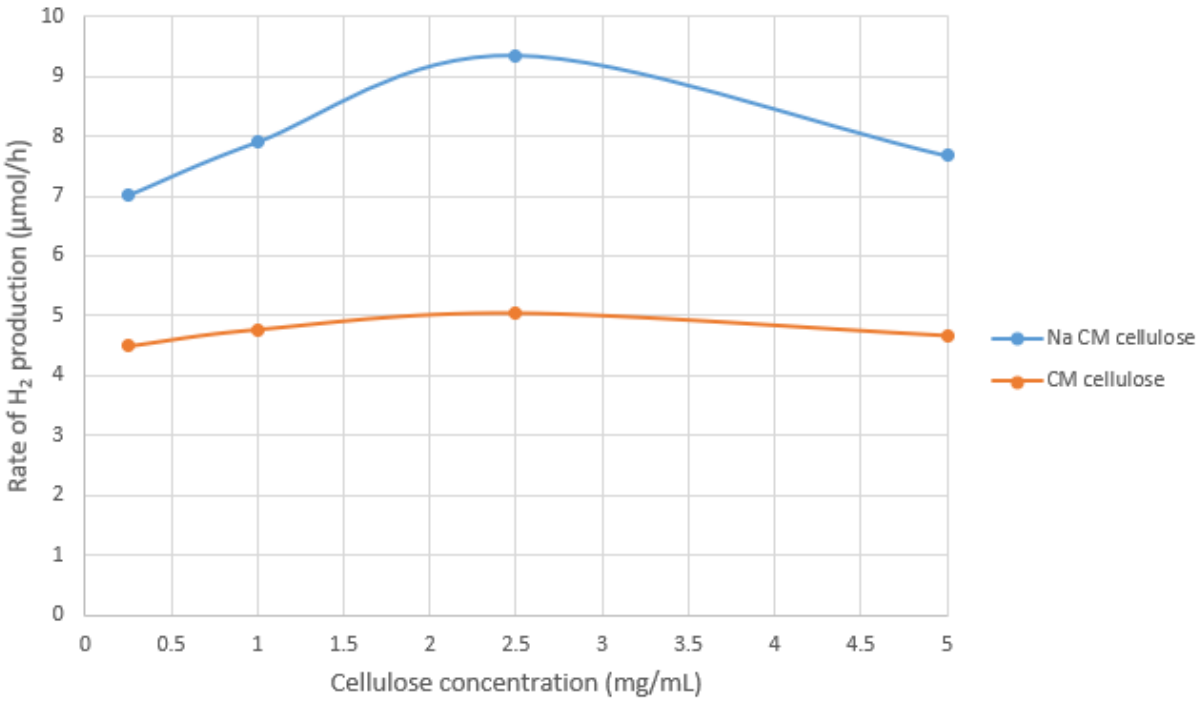

Figure 29: Influence of cellulose concentration on the H_2 rate of production.

The figure shows how, for both types of cellulose, an optimum exists at 2.5 mg/mL. The existence of an optimum can be explained considering two concurrent effects that occur when the concentration of cellulose is increased. On the one hand, as it is generally true for any chemical reaction, an increase of the concentration of reactants translates into an increase in the rate of generation of products, in this case H_2. On the other hand, increasing the concentration of cellulose implies an increase of the shadowing effect of photocatalyst particles from cellulose particles, reducing the amount of photons useful to generate photoexcited electrons and holes. These two opposite tendencies result in the

existence of the optimum mentioned above, that occurs around the same concentration for both the cellulose types tested.

The influence of photocatalyst concentration has also been assessed, varying it between 0.1 and 2 mg/mL at a constant concentration of cellulose equal to 0.25 mg/mL and using Na CM cellulose. Figure 30 summarizes the results obtained, both in terms of total H_2 production and in terms of production normalized with respect to the mass of photocatalyst used.

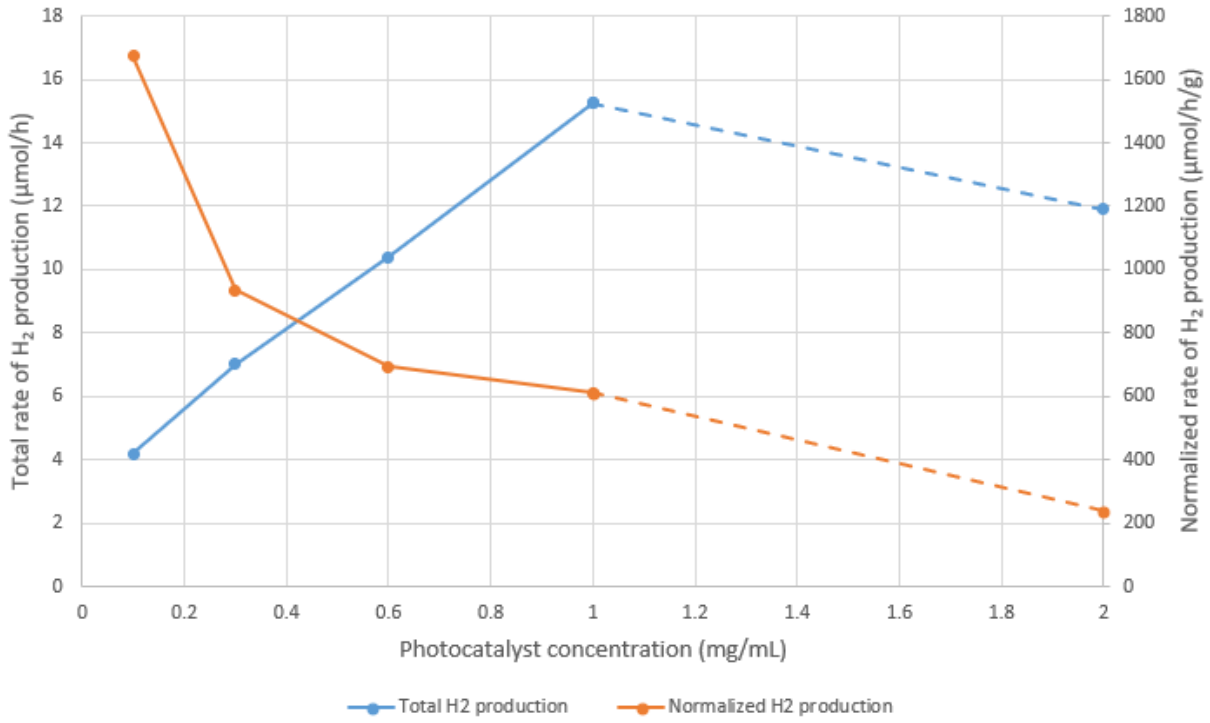

Figure 30: Influence of photocatalyst concentration on the total H_2 production (left axis) and H_2 production normalized with respect to the mass of photocatalyst (right axis).

It is possible to first appreciate how the total production increases with the concentration when this is varied between 0.1 and 1 mg/mL, and how it then decreases when moving to 2 mg/mL. It thus seems that, similarly to what has been shown for cellulose, increasing the concentration of photocatalyst initially brings an advantage as more light can be absorbed and used to produce H_2. When instead the concentration exceeds a certain value, most of the light beam is likely absorbed or scattered by the portion of photocatalyst closer to the light source, so that the rest of the photocatalyst works in non-optimal lighting conditions that decrease the overall production. Also in this case it is possible to show the existence of a concentration that maximizes the production given the working conditions of the experiments.

It has to be noted that the concentrations of photocatalyst and cellulose that maximize the production are most probably dependent on a bunch of factors such as the geometry of the reactor, the lighting conditions and the photocatalyst and cellulose type used. A change in one of these factors may result in a change of the optimal values. The analysis here reported thus only applies to the conditions mentioned, and does not aim at providing absolute values but rather qualitatively showing in what way the concentrations influence the performances.

Figure 30 also allows to see how the rate of production normalized with respect to the mass of photocatalyst used always decreases when the concentration is increased, despite the total production actually increasing. Two operational strategies can therefore be highlighted for such a photocatalytic system, one aiming at maximizing the total production, the efficiency of utilization of the light source and of the space available through higher concentrations, and one aiming at maximizing how effectively each mass unit of photocatalyst is used through lower concentrations. The best compromise probably lies in the middle, and depends on key factors such as the cost of the photocatalyst.

Further experiments have been performed, again with Na CM cellulose, to observe the behavior of the system at a different, constant concentration of photocatalyst and variable concentration of cellulose. A concentration of photocatalyst equal to 1 mg/mL was chosen, being this the value that led to the highest total production among the ones tested. Figure 31 shows, in the same graph, the total production at different cellulose concentrations, and at photocatalyst concentrations of 0.3 and 1 mg/mL.

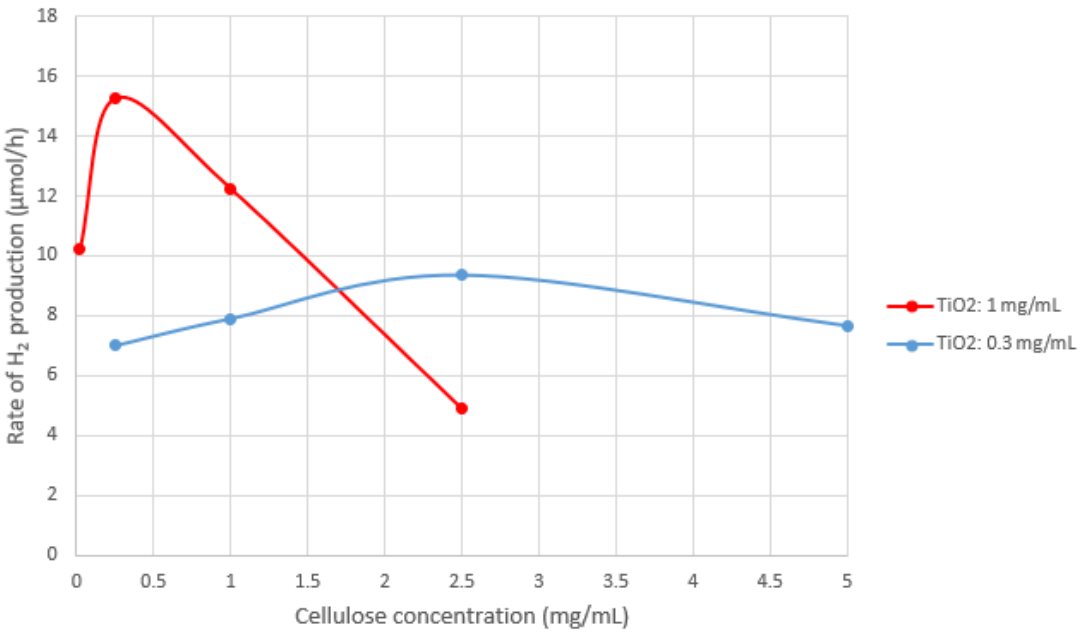

Figure 31: Influence of cellulose concentration on total production at photocatalyst concentrations of 0.3 and 1 mg/mL.

The behavior highlighted in Figure 31 may seem counter-intuitive. Indeed, it could have been expected that a higher concentration of photocatalyst would have allowed to degrade more cellulose, shifting the curve up and to the right. Reality proved instead to be different, with the highest performances in terms of production reached with a higher concentration of photocatalyst and a much lower concentration of cellulose, and a general shift of the curve up-left. Even the lowest concentration of cellulose tested, equal to 0.02 mg/mL, led to decent performances. A possible reason is that, at a higher concentration of photocatalyst, the transparency of the water is already dramatically reduced, implying that lower concentrations of cellulose are needed to allow the light to irradiate all or most of the suspension. When 1 mg/mL of photocatalyst and 2.5 mg/mL of cellulose were tested, indeed, the solution was too dark, leading to the worst performances. The most favorable conditions to maximize the total production are thus a considerable amount of photocatalyst degrading a little quantity of cellulose.

Finally, Figure 32 shows the same graph but with reference to the production normalized with respect to the mass of photocatalyst.

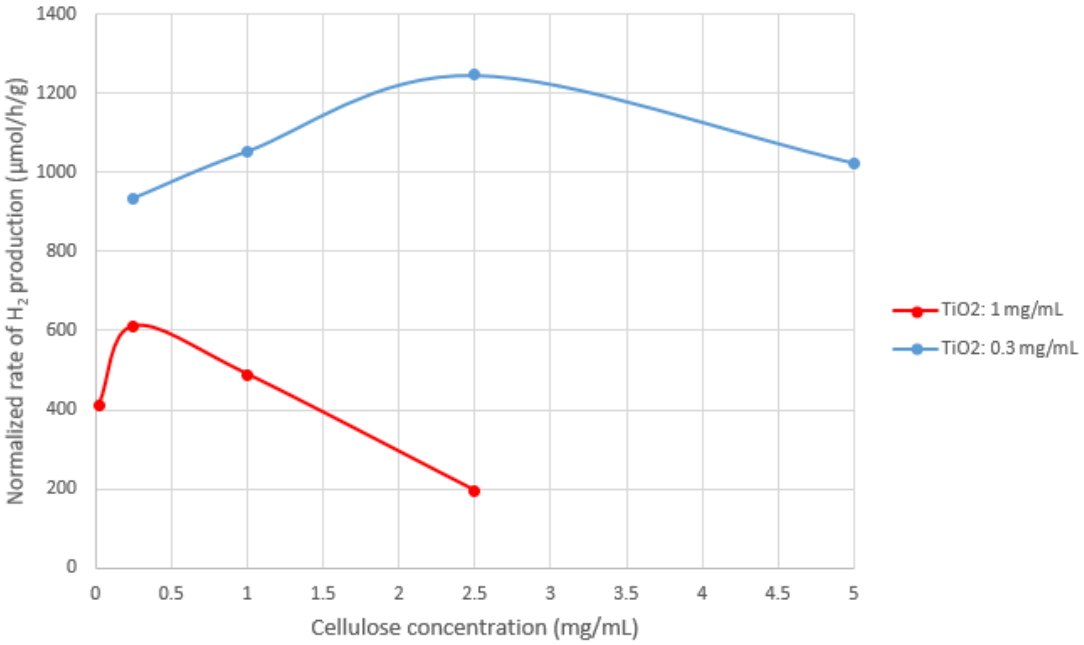

Figure 32: Influence of cellulose concentration on normalized production at photocatalyst concentrations of 0.3 and 1 mg/mL.

In this case, any point at photocatalyst concentration 0.3 mg/mL exploits the material better than any point at 1 mg/mL, suggesting that the trend of lower concentration for higher specific production remains true regardless of the concentration of cellulose.

10.5 Study of pH

This section investigates the influence of suspension's pH on the performances of the system. Before each experiment, the pH was adjusted to the desired value using HCl and NaOH.

It was observed that, whenever starting from a pH higher than 5 (maximum pH tested was 10), at the end of the experiments a pH of 5 was always measured. It thus seems that pH 5 represents a sort of steady state pH that the system reaches when starting from a higher pH. This can be explained keeping in mind the products involved in the degradation chain of cellulose, described in Section 4. Namely, formic acid (HCOOH) and CO_2 are produced, both possibly responsible for the pH decrease of the system. Formic acid contributes to the acidification dissociating into H^+ and $HCOO^-$, and CO_2 by firstly reacting with water forming H_2CO_3 and then dissociating in H^+ and HCO_3^- [47]. The two acids, however, do not seem to be strong enough to lead the pH to values lower than 5, meaning that when a concentration of protons corresponding to pH 5 is reached, no further dissociation occurs. Any pH equal or higher than 5 should then lead to similar performances, being 5 the steady state pH reached after few minutes regardless of the initial conditions.

The situation changes when a pH lower than 5 is used. When the initial pH was adjusted to any value lower than 5, the same value was measured at the end of the experiment. The system is thus unable to alter its concentration of protons when this is equal or higher than 10^{-5} M. The results obtained at different pH values are summarized in Figure 33.

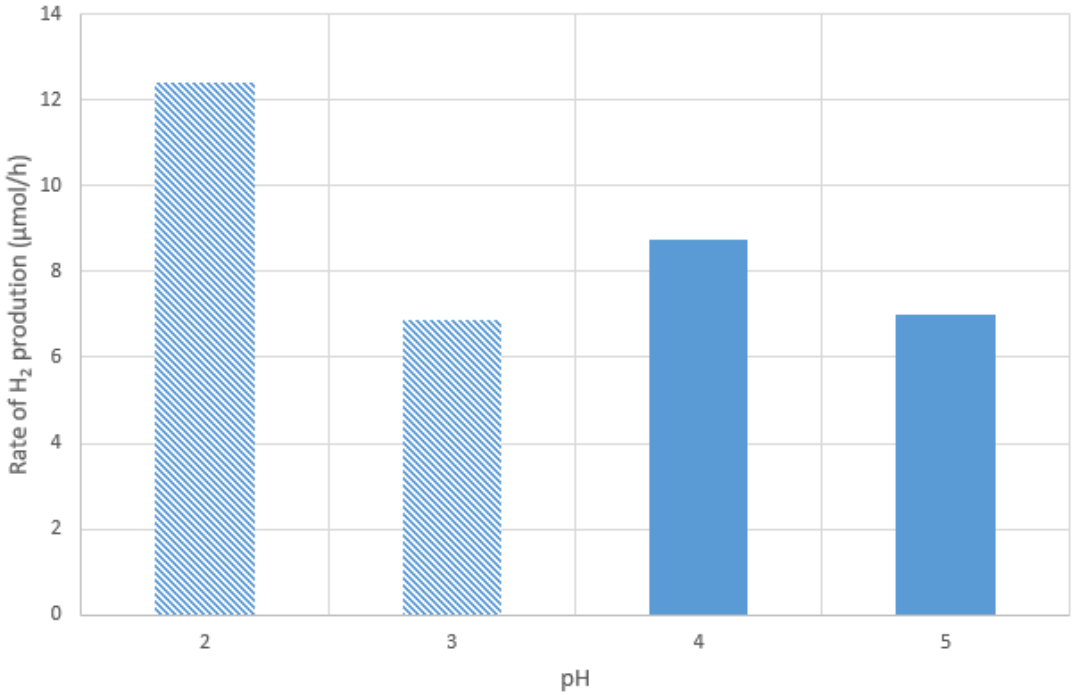

Figure 33: Influence of pH on H_2 production. Dashed columns indicate unstable suspension.

Figure 33 shows an increase of H_2 production moving from pH 5 to pH 4. When the pH was equal to 2 or 3, however, the suspension was unstable and agglomeration of particles was observed. Thus, for those cases, the figure only shows with dashed columns the initial rate of H_2 production, that however almost doubled switching from pH 5 to pH 2. Afterwards, as the agglomeration becomes more severe, the rate of production decreases to almost 0.
What these results seem to suggest is that a low pH is in principle beneficial for the performances of the system, possibly due to more favorable thermodynamic conditions for H_2 evolution: as Figure 6 shows, a lower pH value is associated to a less negative potential needed for reduction of protons. However, at pH 3 or lower the suspension becomes unstable, canceling the effect of the more favorable thermodynamics.

In order to understand why the solution becomes unstable at low pH, it is useful to look at the zeta potential of Na CM cellulose, shown in Figure 34.

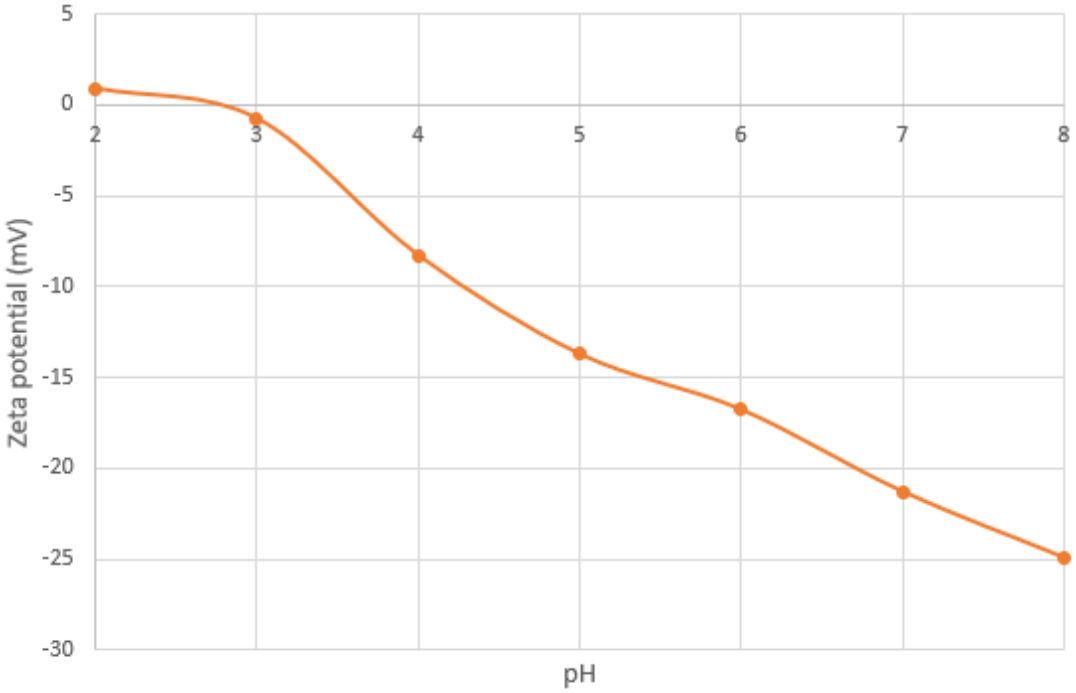

Figure 34: Measured zeta-potential of Na CM cellulose.

It is possible to observe a quite negative zeta potential for pH 4 or higher, indicating a negative net charge on cellulose particles able to prevent their agglomeration. However, at pH 2 and 3, particles have a net charge close to 0, making the suspension unstable and enabling for agglomeration. This explains the results obtained for the experiments at pH 2 and 3. It is interesting to note that, despite a negative zeta potential for cellulose at pH 4 and 5, and a positive zeta potential for TiO_2 nanoparticles, no agglomeration occurs, as instead happens for rapeseed cellulose. The reason is probably the much smaller size of Na CM cellulose particles.

Based on the observations reported in this section, it is possible to conclude that an acidic pH is beneficial for H_2 evolution, provided that the suspension is stable. The stability of the suspension is dependent on the type of cellulose involved and its zeta potential at different pH values. In the case of Na CM cellulose, pH 4 seems to represent the optimal condition.

10.6 Estimation of efficiency

This sections aims at estimating the efficiency of the system, when Na CM cellulose is used as sacrificial agent, at the values of concentrations and pH that in the previous sections led to the best performances among the ones tested, namely:

•Photocatalyst concentration: 1 mg/mL;
•Cellulose concentration: 0.25 mg/mL;
•pH: 4.

The type of efficiency analyzed is the light-energy-to-hydrogen-energy conversion efficiency (LHCE), that compares the energetic content of the H_2 produced to the energy of the light beam shining on the reactor. The LHCE can be expressed as follows [48]:

$$\eta_{LHCE}(\%) = 100\frac{(\Delta G^0 - RTln(p_0/p))R_{H_2}}{E_s A} \tag{6}$$

where ΔG^0 is the change of Gibbs free energy for the water splitting reaction at 25 °C and 1 atm, equal to 237200 J/mol, R is the universal gas constant, T the absolute temperature equal to 313 K, p_0 the atmospheric pressure and p the operating pressure, measured by the sensor, R_{H_2} the rate of H_2 generation in mol/s, E_s the intensity of the light shining on the reactor, equal to 1000 W/m^2, and A the area exposed to the light.
Three different experiments were done to determine the rate of H_2 production production R_{H_2}. In order to account for the area, the reactor was covered with aluminium foil where a circular window with a 2.2 cm diameter was designed. Table 2 shows the rate of H_2 production and efficiency obtained in each experiment:

Table 2: STH efficiency values for various experiments

Experiment	R_{H_2} (μmol/s)	η_{LHCE} (%)
1	0.00252	0.14
2	0.00258	0.15
3	0.00245	0.14

All three experiments led to quite similar outcomes, that indicate a LHCE around 0.14-0.15 %. This value is fairly low, especially if compared to the value required for commercial feasibility, around 10 % [49]. Such a low conversion of light energy to H_2 energy indicates that efforts are necessary to synthesize a material able to exploit more efficiently the light source. As Figure 16 shows, the photocatalyst used in the experiments significantly absorbs light only for wavelengths much lower than 400 nm, an extremely small part of the solar spectrum characterized by a higher probability to be absorbed by the glass of the reactor without even reaching the suspension. Moreover, it is reported that even if all the UV light of the solar spectrum with wavelength up to 400 nm could be used, the LHCE would still be as low as 2 % [22]. For these reasons, attempts to prepare a material with improved absorption of light have been done and described in Section 10.8.

10.7 Comparison with other sacrificial agents

This section reports a comparison of the performances enabled by Na CM cellulose with those enabled by other sacrificial agents. Sodium sulfide enneahydrate ($Na_2S{\cdot}9\ H_2O$), glucose and methanol have been considered. For Na CM cellulose, glucose and sodium sulfide the concentration used was 0.25 mg/mL, while methanol was exmplyed with a concentration of 1 mL in 25 mL, corresponding to approximatively 0.1 mM. The concentration of photocatalyst was 0.3 mg/mL for every experiment, while the natural pH was left for the new sacrificial agents. Figure 35 shows the rates of production obtained.

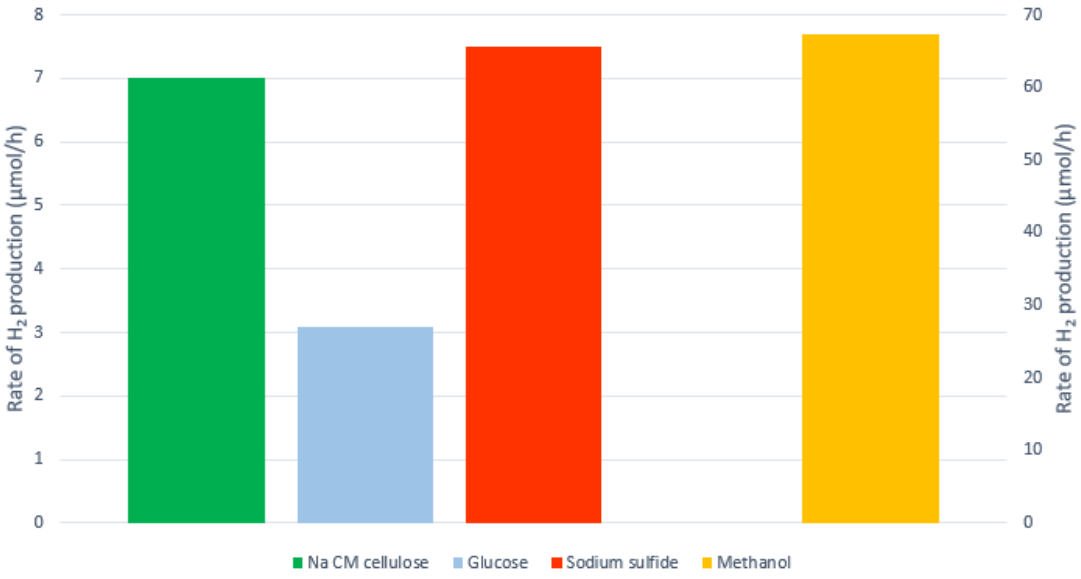

Figure 35: Comparison with other sacrificial agents. Na CM cellulose, glucose and sodium sulfide on left axis, methanol on right axis.

Surprisingly, at the conditions studied, Na CM cellulose allowed a production two times higher than that obtained with glucose. When glucose was used, indeed, agglomeration of particles occurred. Different initial pH values did not change significantly the outcome. A possible explanation is that glucose acted as a bridging element, with same glucose molecules being adsorbed on the surface of several TiO_2 particles. The results obtained with sodium sulfide is instead comparable to that obtained with Na CM cellulose. The production of H_2 obtained with methanol as sacrificial agent is significantly higher. This experiment is the one that led to the highest rate of production in the whole study, corresponding to a normalized value of 8956 μmol/(h·g). However, as mentioned earlier, methanol is already a valuable fuel, making it pointless to use it for conversion to H_2.

For comparison, an estimation of the LHCE with methanol as sacrificial agent was performed. A photocatalyst concentration of 0.3 mg/mL and a methanol concentration of 1 mL in 25 mL were used. The procedure used for the estimation is the same described in

Subsection 10.6. The result obtained is an efficiency of 0.63 %. Despite the improvement compared to the conversion efficiency with Na CM cellulose (0.15 %), the efficiency is still below 1 %, suggesting that much higher performances are required from the photocatalyst side.

To summarize, Na CM cellulose behaves, at same mass concentration, better than or similarly to other well-known sacrificial agents which are not already a fuel, despite being, at the same time, a derivative of the most abundant polymer on earth. This proves its great potential as sacrificial agent for photocatalytic production of H_2.

10.8 Comparison with other photocatalysts

With the aim of achieving better performances and improve the absorption of light, 3 Z-schemes involving g-C_3N_4 are here proposed. In order to be suitable to degrade cellulose, the photocatalyst must be able to generate $OH^\bullet$ radicals through the water oxidation mechanism reported in Equation 2, while still being in condition to reduce protons with evolution of H_2.

All the experiments reported in this section refer to a photocatalyst concentration of 0.3 mg/mL and a concentration of Na CM cellulose of 0.25 mg/mL. Any other parameter such as light intensity has been left unchanged.

10.8.1 TiO_2/g-C_3N_4 heterojunction

The first Z-scheme proposed still involves TiO_2. Several previous studies report the possibility of a direct Z-scheme composed by TiO_2 and g-C_3N_4 ([23], [50]). The main goal of this type of junction is not increasing the absorption of visible light, since TiO_2 would still act as a bottle neck, but rather exploiting the improved separation of charges promoted by the Z-scheme. The junction is schematically depicted in Figure 36, in which it is possible to appreciate holes in the TiO_2 phase and electrons in the g-C_3N_4 phase.

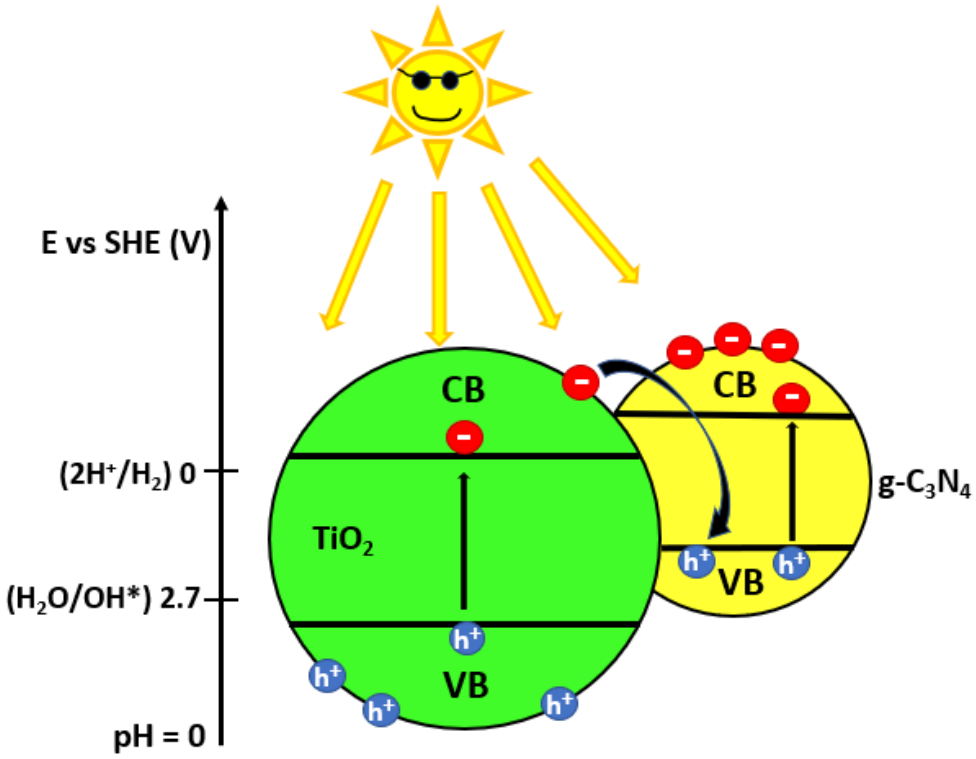

Figure 36: Schematic representation of TiO_2/C_3N_4 Z-scheme.

Yu et al. [50] employed this kind of junction to degrade formaldehyde, reporting a faster degradation with respect to the case in which pure TiO_2 was used. A TiO_2/g-C_3N_4 heterojunction was thus prepared through a procedure similar to that followed by Yu et al. Briefly, a 30 mL suspension containing 300 g of P25 and 300 g of urea was ultrasonicated and stirred for 3 h, with urea being the g-C_3N_4 precursor. The 1:1 mass ratio between P25 and urea has been chosen as it led to the best performances in the study conducted by Yu et al. After drying the suspension at 60°C, the resulting powder was ground and heated in a crucible with cover at 550 °C for 1 h., with a heating ramp of 10 °C/min.

The enhanced charge separation allowed by the Z-scheme has been proved by measuring the concentration of $OH^\bullet$ radicals using TPA, with a procedure analogous to that used in Subsection 10.2 and better clarified in Appendix 2. Two samples were prepared by suspending P25 TiO_2 and the synthesized TiO_2/g-C_3N_4, with a concentration of 0.2 mg/mL, in 25 mL of a 500 μM TPA solution. The samples were then irradiated for 5 min and the respective emissions, caused by the hTPA generated when light was shined, were observed by PL spectroscopy. The obtained emission intensities and the corresponding concentration of $OH^\bullet$ radicals are displayed in Table 3.

The table shows a 3-fold increase in the concentration of $OH^\bullet$ radicals when g-C_3N_4 is added, attesting the enhanced separation of charges allowed by the Z-scheme.

Table 3: Emission intensity of hTPA and concentration of $OH^{\bullet}$ radicals for P25 and TiO_2/g-C_3N_4.

Material	Emission intensity	$[OH^{\bullet}]$ (M)
P25	118.9	$1.82 \cdot 10^{-15}$
TiO_2/g-C_3N_4	334.4	$5.41 \cdot 10^{-15}$

The UV-vis absorption spectrum displayed in Figure 37 reveals instead a decrease of the absorption in the UV range accompanied by an increase in the visible region.

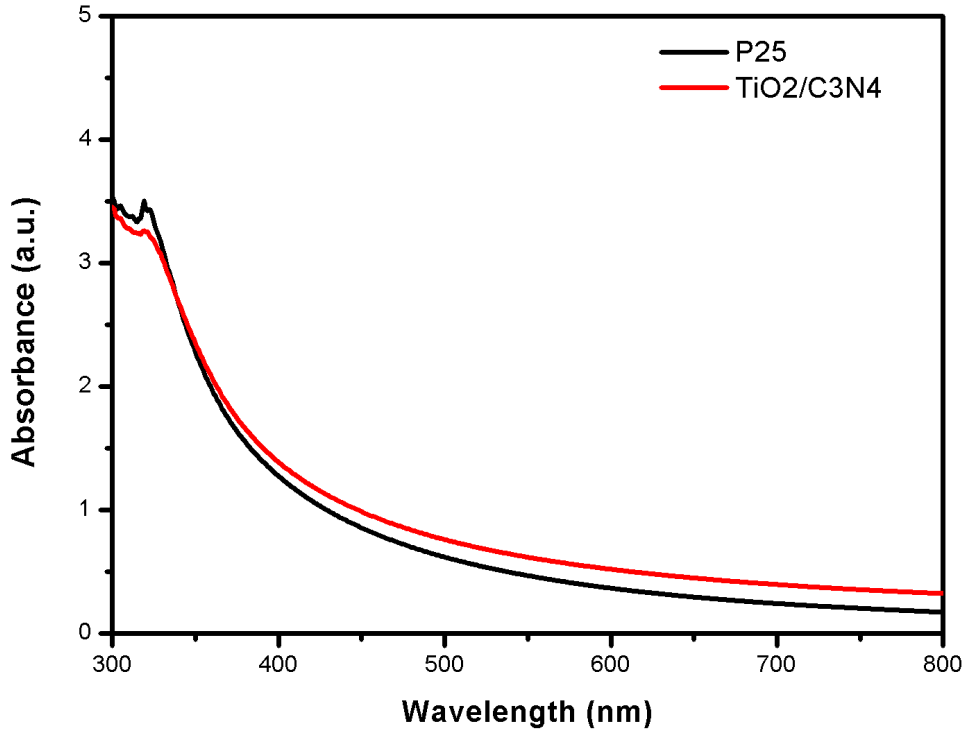

Figure 37: Light absorbance of P25 TiO_2 and TiO_2/g-C_3N_4.

The material was then tested for H_2 generation. Though a modest generation of H_2 could be observed when testing the material without any noble metal cocatalyst, Pt deposition was necessary to achieve a considerable rate of production. Pt was therefore deposited according to the procedure clarified in Subsection 7.1, with a 0.5 % mass loading. Despite all the encouraging characteristics shown above, the rate of H_2 generation observed was equal to 3.5 μmol/h, approximatively half of the rate observed when TiO_2/Pt 0.5 % was used at the same conditions.

A possible explanation is that the interface with g-C_3N_4 does help to achieve separation of charges but, when Pt is deposited, it enables a better result bypassing the beneficial effect of the g-C_3N_4 phase. Consequently, having only TiO_2 may represent a more convenient situation, as all the material introduced in the system is functional to the production of $OH^{\bullet}$ radicals and separation of charges is ensured by Pt nanoparticles.

The other Z-schemes tried, therefore, mostly aim at enhancing the performances by using materials with smaller band gaps and increased light absorption.

10.8.2 Ag_3PO_4/N-GQDs/g-C_3N_4 heterojunction

The second Z-scheme proposed involves Ag_3PO_4 for oxidation of water and g-C_3N_4 for reduction of protons. With suitable band gap positions, whose values are respectively 2.45 [51] and 2.7 eV [23], the material would theoretically allow to absorb light up to about 500 nm. In this case, N-doped graphene quantum dots (N-GQDs) were added as a conductive interface between the two materials, in order to facilitate the transfer of charges. A schematic representation is provided in Figure 38.

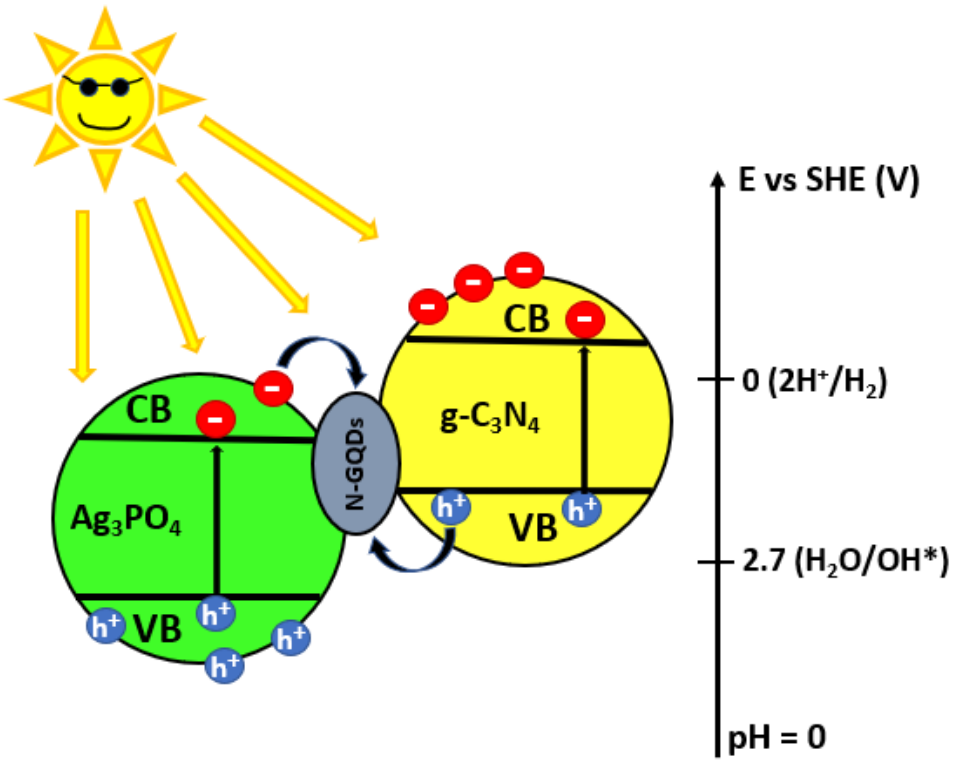

Figure 38: Schematic representation of Ag_3PO_4/g-C_3N_4 Z-scheme.

Ag_3PO_4 particles were prepared following the procedure explained by Batvandi et al. [52]. 0.318 g of $AgNO_3$ were dissolved in 32 mL of DI water, and 41 μL of orthophosphoric acid were added at a rate of 1 drop every 3 seconds. 0.197 g of hexamethylenetetramine (HMT) were then added, followed by 15 minutes of magnetic stirring. The obtained product was centrifuged and dried.

g-C_3N_4 sheets were prepared in a two steps process followed by thermal treatment and liquid exfoliation ([53], [54]). 5 g of melamime were heated at 520 °C in a crucible with cover for 4 hours, with a ramping rate of 5 °C/min. The obtained product was ground and heated again at 520 °C for 2 hours, with a ramping rate of 2 °C/min. An exfoliation process followed, according to which 1 g of g-C_3N_4 was dispersed in 50 mL of concentrated H_2SO_4 and kept for 6 hours under ultrasonication. The resultant suspension was washed with DI water until being adjusted to pH 7, and the obtained product was dispersed in 50 mL of ethanol and stored at 5 °C.

N-GQDs were prepared by dissolving 2 g of ammonium citrate tribasic in 40 mL of DI water and refluxed at 200 °C for 30 mins. The obtained suspension adjusted to pH 7 and stored at 5 °C.

The Ag_3PO_4/N-GQDs/g-C_3N_4 was obtained following a refluxing technique reported in literature [53]. 1 g of as prepared powder were dispersed in 30 mL of N-GQDs suspension by 1 h ultrasonication, then stirring for 6 h and vacuum freeze drying. The remaining powder was suspended in 15 mL of g-C_3N_4 suspension and ultrasonicated for 1 h. The resulting suspension for kept at 65 °C under reflux overnight, then the condenser was removed until complete evaportation of the ethanol. The wet precipitate was kept in the oven at 60 °C for 3 h and finally ground.
Figure 39 displays the light absorbance that has been measured for the material, with an interesting peak in the visible region.

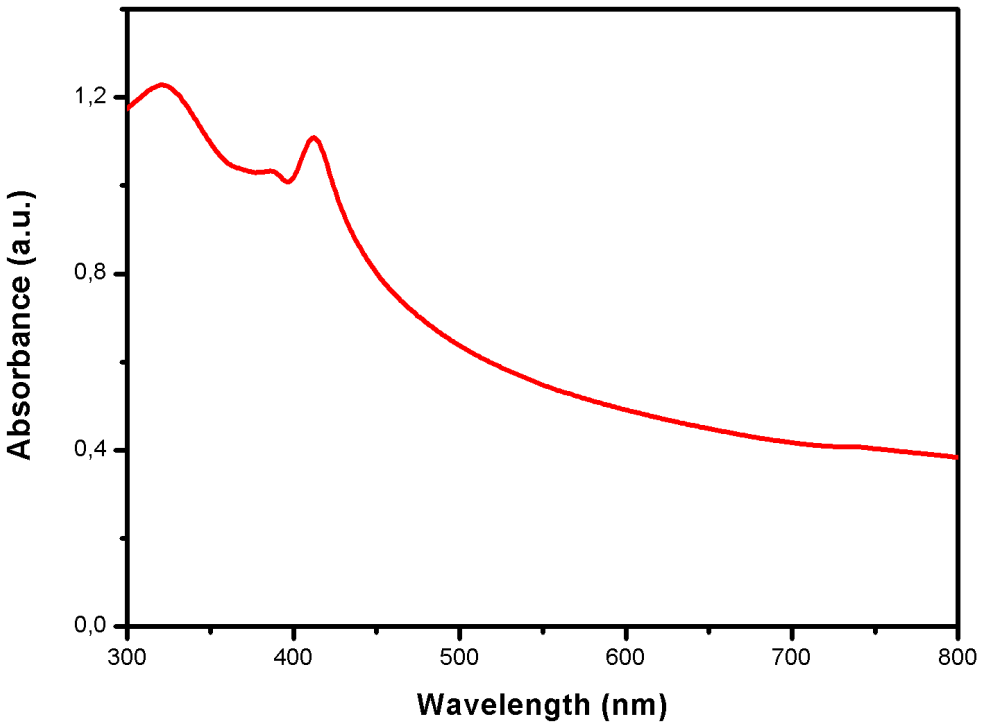

Figure 39: Light absorbance of Ag_3PO_4/g-C_3N_4 Z-scheme.

After deposition of Pt with a mass loading of 0.5 %, according to the procedure reported in Subsection 7.1, the photocatalyst was tested for H_2 prodection. Unfortunately, no H_2 has been produced, most probably due to issues during the preparation of the material yet not well clarified.

10.8.3 WO_3/g-C_3N_4 heterojunction

The last Z-scheme proposed involves WO_3 for water oxidation reaction and g-C_3N_4 for reduction of protons. With a band gap of 2.7 eV for both g-C_3N_4 and WO_3 ([23], [27]), the material is expected to allow an increase of light absorption with respect to TiO_2. A schematization of the material has already been provided in Figure 13, that shows how the positions of the band gaps are suitable for generation of $OH^{\bullet}$ radicals and H_2 evolution.

The photocatalyst was prepared according to the following procedure. At first, WO_3 nanoaprticles have been prepared according to the method explained by Martinez-de la Cruz et al. [55]. 0.00107 mol of ammonium tungstate hydrate have been dissolved in 67 mL of DI water at 80 °C. 45 mL of concentrated HNO_3 have then be added dropwise. The solution was kept for 40 mins under stirring at 80 °C, and was then allowed to settle

for 1 day at room temperature. The precipitate was collected and dried in oven at 80 °C overnight and finally thermally treated at 400 °C for 40 mins.

g-C_3N_4 nanosheets were prepared by keeping urea at 550 °C for 2.5 h in a crucible with cover. The obtained material was then ground into fine powder and annealed at the same temperature for 1 h.

The WO_3/g-C_3N_4 composite was prepared following a procedure similar to that reported by Yang et al. [56]. WO_3 and g-C_3N_4 were suspended in methanol and stirred for 24 h. Different mass ratios of the two types of particles were tested. After volatilization of methanol, the particles were dried overnight at 80 °C and calcinated at 400 °C for 2 h.

The obtained powders were tested for H_2 production with methanol as sacrificial agent and without any noble metal deposition, showing that a mass ratio of 1:1 leads to the best performances. Figure 40 shows the light absorption of the 1:1 WO_3/g-C_3N_4 photocatalyst, that also in this case reaches the visible region.

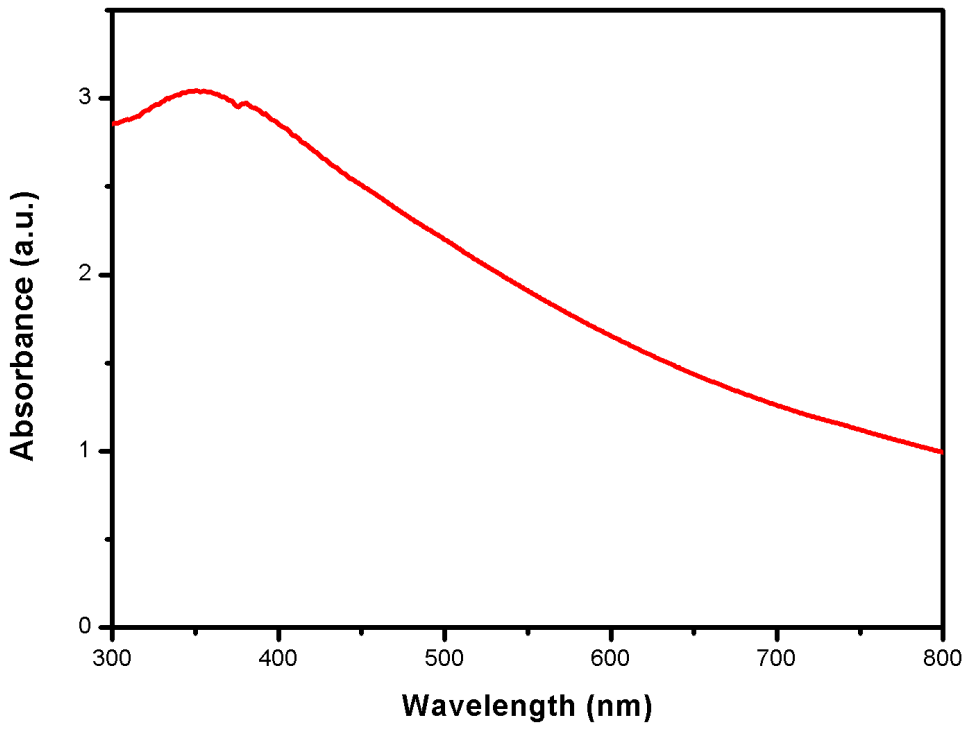

Figure 40: Light absorbance of WO_3/g-C_3N_4 Z-scheme.

WO_3/g-C_3N_4 with 1:1 mass ratio was thus decorated with Pt nanoparticles with a mass

loading of 0.5 % and tested for H_2 generation using Na CM cellulose as sacrificial agent. The rate of H_2 obtained was 2 μmol/h, still less than half of that obtained with TiO_2/Pt 0.5 % at the same conditions.

Since the preparation of a good photocatalyst is a complex process that requires experience and time, no further attempts were made within the short time available for this study. The current lack of an estimation of the efficiency with a photocatalyst able to absorb in the visible range, when cellulose is used as sacrificial agent, gives room for further research.

11 Sustainability aspects

A successful deployment of photocatalytic generation of H_2 from cellulose would have several positive effects that can be listed in relation to some relevant Sustainable Development Goals [57]. Firstly, since the process represents a way to convert into fuel solar energy and the chemical energy contained in cellulose molecules, both being renewable and abundant forms of energy, it would be helpful to achieve the SDG 7, Affordable and clean energy. The deployment of the technology would then boost local economies, industries, labour, and research, contributing simultaneously for the achievement of SDG 8, Decent work and economic growth, and SDG 9, Industry, innovation and infrastructure. The SDG 11, Sustainable cities and communities, would also be pursued, as the carbon footprint of communities using the technology would be reduced. Finally, because of the reduction of CO_2 emissions allowed, the technology would contribute in slowing down the ongoing climate change in accordance to the SDG 13, Climate action. Figure 41 summarizes the SDGs involved.

Figure 41: SDGs related to the present study [57].

Possible issues may arise when it comes to the photocatalyst used, that should allow a good

efficiency while being affordable enough, without posing any significant environmental threat throughout all its life cycle.

12 Validity, reliability, replicability, scalability

The validity of the present study is ensured by the relevance of the topic investigated, well fitting in the current framework of climate emergency, in which alternative, low carbon emitting energy sources and fuels are needed.
Because of the short time span available for the study, it was not possible to repeat several times every single experiment. Some key experiments, however, have been repeated multiple times in order to still confer a good reliability to the observations made. Every time an experiment was repeated the results obtained were quite close to each other, suggesting a reasonable intrinsic acceptability.
Since every step performed is carefully described, the replicability of the study is guaranteed and any researcher is in condition to repeat the experiments.
When performing the same study at a different scale, it is expected that, qualitatively, the trends shown are kept, though numeric results and positions of optima would most probably change.

13 Conclusions

This study investigated the possibility of photocatalytic H_2 generation using cellulose as sacrificial agent, being an innovative way to produce an environmentally friendly fuel of renewable origin. By employing TiO_2/Pt as photocatalyst, different types of cellulose were tested, highlighting how cellulose types with lower crystallinity index and cellulose derivatives containing CH_2COOH, CH_2COONa and COONa groups are most suitable for the application. It was shown how the concentrations of photocatalyst and cellulose influence the performances. Namely, a "high" concentration of photocatalyst and a "low" concentration of cellulose represent the optimal configuration to maximize the rate of H_2 production. The pH of the reaction medium was demonstrated to be another key parameter, with low pH values that, on the one hand, are helpful for H_2 evolution, but, on the other hand, hinder the stability of the suspension. A comparison with other sacrificial agents showed how cellulose enables better performances than glucose at the tested conditions, while considerably higher rates of production can be achieved when methanol is employed, which is however a much more expensive option. The low light-energy-to-hydrogen-energy conversion efficiency (LHCE), estimated around 0.15 %, motivated the research of a new photocatalyst able to better exploit the light resource. Three suitable Z-scheme photocatalysts were tested, namely TiO_2/g-C_3N_4, Ag_3PO_4/N-GQDs/g-C_3N_4 and WO_3/g-C_3N_4. While TiO_2/g-C_3N_4 and WO_3/g-C_3N_4 showed a worsening of the performances, no useful result could be obtained with Ag_3PO_4/N-GQDs/g-C_3N_4, most probably due to issues in the preparation process. Further research can be done to estimate the

LHCE with a photocatalyst able to absorb in the visible region, using a cheap, abundant and promising sacrificial agent such as cellulose.

References

[1] Paris Agreement, United Nations Framework Convention on Climate Change (2015), https://unfccc.int/process-and-meetings/the-paris-agreement/the-paris-agreement

[2] International Energy Agency, www.iea.org

[3] Lindsey R., "Climate Change: Atmospheric Carbon Dioxide", Climate.gov (2020), https://www.climate.gov/news-features/understanding-climate/climate-change-atmospheric-carbon-dioxide#:~:text=Carbon%20dioxide%20levels%20today%20are,least%20the%20past%20800%2C000%20years.&text=Global%20atmospheric%20carbon%20dioxide%20concentrations,interglacials%20(higher%20CO2).

[4] Calise F. et al., "Detailed Modelling of the Deep Decarbonisation Scenarios with Demand Response Technologies in the Heating and Cooling Sector: A Case Study for Italy", Energies (2017), 10(10), 1535

[5] Lassila J. et al., "Network Effects of Electric Vehicles - Case From Nordic Country", CIRED International Conference on Electricity Distribution (2011), 0773

[6] Mrozik W. et al., "Environmental impacts, pollution sources and pathways of spent lithium-ion batteries", Energy Environmental Science (2021), 14, 6099-6121

[7] "Hydrogen Resources", Energy.gov, https://www.energy.gov/eere/fuelcells/hydrogen-resources

[8] O'Neil S., "Unlocking the Potential of Hydrogen Energy Storage", FCHEA Fuel Cell Hydrogen Energy Association (2019), https://www.fchea.org/in-transition/2019/7/22/unlocking-the-potential-of-hydrogen-energy-storage#:~:text=Hydrogen%20energy%20storage%20is%20a,in%20order%20to%20separate%20hydrogen.

[9] Sun S. et al., "The role of pretreatment in improving the enzymatic hydrolysis of lignocellulosic materials", Bioresource Technology (2016), 199, 49-58

[10] Nave R., "Band Theory of Solids", HyperPhysics http://hyperphysics.phy-astr.gsu.edu/hbase/Solids/band.html

[11] Siahrostami S. et al., "One- or Two-electron Water Oxidation, Hydroxyl Radical or H_2O_2 Evolution", The Journal of Physical Chemistry Letters (2017), 8, 6, 1157–1160

[12] Caravaca A. et al., "H_2 production by the photocatalytic reforming of cellulose and raw biomass using Ni, Pd, Pt and Au on titania", Proceedings of the Royal Society A (2016), 472, 2191

[13] Wieserma B.J., "Alternative and Enhanced Chemical Cleaning: Corrosion Studies Results: FY2010", Materials Science (2010)

[14] Tamirat A. G., "Using hematite for photoelectrochemical water splitting: a review of current progress and challenges", Nanoscale Horizons, 2016

[15] Fujishima A., Honda K., "Electrochemical Photolysis of Water at a Semiconductor Electrode", Nature (1972), 238, 37-38,

[16] Singh R., Dutta S., "Integrated photocatalytic hydrogen production and pollutants or wastes treatment: prospects and challenges", Sustainable Fuel Technologies Handbook (2021), 541-549

[17] Chong et al., "Selective conversion of aqueous glucose to value-added sugar aldose on TiO2-based photocatalysts", Journal of Catalysis (2014), 314, 101-108

[18] Speltini A. et al., "Sunlight-promoted photocatalytic hydrogen gas evolution from water-suspended cellulose: a systematic study", Photochemical Photobiological Sciences (2014), 13, 1410-1419

[19] Wu G., Chen, T., Zhou, G. et al., "H2 production with low CO selectivity from photocatalytic reforming of glucose on metal/TiO2 catalysts", Science in China Series B: Chemistry (2008), 51, 97–100

[20] Fu X. et al., "Photocatalytic reforming of biomass: A systematic study of hydrogen evolution from glucose solution", International Journal of Hydrogen Energy (2008), Volume 33, Issue 22, Pages 6484-6491

[21] Corredor J. et al., "Comprehensive review and future perspectives on the photocatalytic hydrogen production", Journal of Chemical Technology and Biotechnology (2019), 94, 3049-3063

[22] Abe R., "Recent progress on photocatalytic and photoelectrochemical water splitting under visible light irradiation", Journal of Photochemistry and Photobiology C: Photochemistry Reviews (2010), 11, 179-209

[23] San Martin S. et al., "Unravelling the Mechanisms that Drive the Performance of Photocatalytic Hydrogen Production", Catalysts (2020), 10, 901

[24] Raza W., Ahmad K., "Chapter 6 - Graphitic carbon nitride-based photocatalysts for hydrogen production", Sustainable Materials and Green Processing for Energy Conversion (2022), 213-236

[25] Xie M. et al., "Hydrogen production by photocatalytic water-splitting on Pt-doped TiO2–ZnO under visible light", Journal of the Taiwan Institute of Chemical Engineers (2017), 70, 161-167

[26] Perez-Larios A. et al., "Improved hydrogen production from water splitting using TiO2–ZnO mixed oxides photocatalysts", Fuel (2012), 100, 139-143

[27] Xing P. et al., "Preparation of WO3/g-C3N4 composites with enhanced photocatalytic hydrogen production performance", Applied Physics A (2019), 125, 788

[28] Du J. et al., "Ag3PO4/g-C3N4 Z-scheme composites with enhanced visible-light-driven disinfection and organic pollutants degradation: Uncovering the mechanism", Applied Surface Science (2021), 541, 148487

[29] Huang F. et al., "Influences of Doping on Photocatalytic Properties of TiO2 Photocatalyst", Semiconductor Photocatalysis - Materials, Mechanisms and Applications (2016)

[30] Deng F. et al., "3 - Nanomaterial-Based Photocatalytic Hydrogen Production", Nanomaterials for the Removal of Pollutants and Resource Reutilization (2019), 59-82

[31] Li Q. et al., "Chapter 10 - Surface and interface modification strategies of CdS-based photocatalysts", Interface Science and Technology (2020), 31, 313-348

[32] Chang C., "Using cellulose polymorphs for enhanced hydrogen production from photocatalytic reforming", Sustainable Energy Fuels (2019), 3, 1971-1975

[33] Wakerley D. et al., "Solar-driven reforming of lignocellulose to H2 with a CdS/CdOx photocatalyst", Nature Energy (2017), 2, 17021

[34] Yao W. et al., "Chemical deposition of platinum nanoparticles on iridium oxide for oxygen electrode of unitized regenerative fuel cell", Electrochemistry Communications (2007), 9, 1029-1034

[35] "Ligning", Wikipedia, https://en.wikipedia.org/wiki/Lignin

[36] Holtzapple M. T., "Cellulose", Encyclopedia of Food Sciences and Nutrition (Second Edition) (2003), 998-1007

[37] Dürig T., Karan K., "Chapter 9 - Binders in Wet Granulation", Handbook of Pharmaceutical Wet Granulation (2019), 317-349,

[38] Kaffashsaie E. et al., "Direct conversion of raw wood to TEMPO-oxidized cellulose nanofibers", Carbohydrate Polymers (2021), Volume 262, 117938

[39] Alavi M., Rai M., "Recent progress in nanoformulations of silver nanoparticles with cellulose, chitosan, and alginic acid biopolymers for antibacterial applications", Applied M

[40] OSRAM, www.osram.com

[41] "Solar radiation", Kipp & Zonen, https://www.kippzonen.com/KnowledgeCenter/Theoretical-info/Solar-Radiation

[42] "Solar Radiation Photosynthetically Active Radiatio", Fondriest, https://www.fondriest.com/environmental-measurements/parameters/weather/photosynthetically-active-radiation/

[43] Page S. et al., "Terephthalate as a probe for photochemically generated hydroxyl radical", Journal of Environmental Monitoring (2010), 12, 1658-1665

[44] Pate K., Safier P., "12 - Chemical metrology methods for CMP quality", Advances in Chemical Mechanical Planarization (CMP) (2016), 299-325

[45] Benz D. et al., "Assessing the Role of Pt Clusters on TiO2 (P25) on the Photocatalytic Degradation of Acid Blue 9 and Rhodamine B", The Journal of Physical Chemistry C (2020), 124, 15, 8269–8278

[46] Kalpakli Y. et al., "Photocatalytic degradation of textile dye CI Basic Yellow 28 wastewater by Degussa P25 based TiO2", Advances in environmental research (2015), volume 4, issue 1, pages 25-38

[47] "Ocean acidification", National Oceanic and Atmospheric Administration, https://www.noaa.gov/education/resource-collections/ocean-coasts/ocean-acidification

[48] Kosourov S. et al., "Evaluation of light energy to H2 energy conversion efficiency in thin films of cyanobacteria and green alga under photoautotrophic conditions", Algal Research (2017), 28, 253-263

[49] Cox C. R. et al., "Ten-percent solar-to-fuel conversion with nonprecious materials", PNAS September 30 (2014), 111 (39), 14057-14061

[50] Yu J. et al., "Enhanced photocatalytic performance of direct Z-scheme g-C3N4–TiO2 photocatalysts for the decomposition of formaldehyde in air", Physical Chemistry Chemical Physics (2013), 15, 16883-16890

[51] Liu J. J. et al., "Electronic structure and optical properties of Ag3PO4 photocatalyst calculated by hybrid density functional method", Appl. Phys. Lett. (2011), 99, 191903

[52] Batvandi M. et al., "Synthesis of Ag3PO4 microstructures with morphology-dependent optical and photocatalytic behaviors", Applied Physics A (2020), 126, 571

[53] Feng C. et al., "Core-shell Ag2CrO4/N-GQDs@g-C3N4 composites with anti-photocorrosion performance for enhanced full-spectrum-light photocatalytic activities", Applied Catalysis B: Environmental (2018), 239, 525-536

[54] Deng Y. et al., "Construction of plasmonic Ag and nitrogen-doped graphene quantum dots codecorated ultrathin graphitic carbon nitride nanosheet composites with enhanced photocatalytic activity: full-spectrum response ability and mechanism insight", ACS Appl. Mater. Interfaces (2017), 9, 42816–42828

[55] Martinez-de la Cruz et al., "Synthesis and characterization of WO3 nanoparticles prepared by the precipitation method: Evaluation of photocatalytic activity under vis-irradiation", Solid State Sciences (2010), 12, 88-94

[56] Jang M. et al., "The influence of preparation method on the photocatalytic performance of g-C3N4/WO3 composite photocatalyst", Ceramics International (2014), 40, 11963-11969

[57] "The 17 Goals", United Nations, https://sdgs.un.org/goals

[58] Unisense, https://unisense.com/

14 Appendices

Appendix 1: Sensor working principle and calibration

The sensor works thanks to a tip containing a membrane and a Pt anode. Pushed by the effect of pressure, some of the H_2 molecules present in the sensing environment will pass through the tip membrane and will be oxidized by the platinum electrode. The oxidation current is then converted into an output voltage signal in mV [58].
With a calibration of the instrument at points with known H_2 concentration, it is possible to translate the voltage output in concentration values in μmol/L. Since the temperature will affect the partial pressure of the gas, and thus the number of atoms that will pass through the tip membrane in the same time amount, the calibration has to be done at the same temperature of the experiments. Temperature is in turn measured thanks to a sensor that follows the same principle, which is already calibrated by the manufacturer to give an output in °C.
Experiments were carried out to figure out the steady state temperature of the location of the gas phase where the sensors were placed. In order to limit the temperature variation and reach reasonably soon a steady state temperature a fan was used to cool down the system. As a result a steady state temperature of around 40 °C was observed. Figure 42 shows the temperature variation observed during one of the experiments at the sensors location in the gas phase.

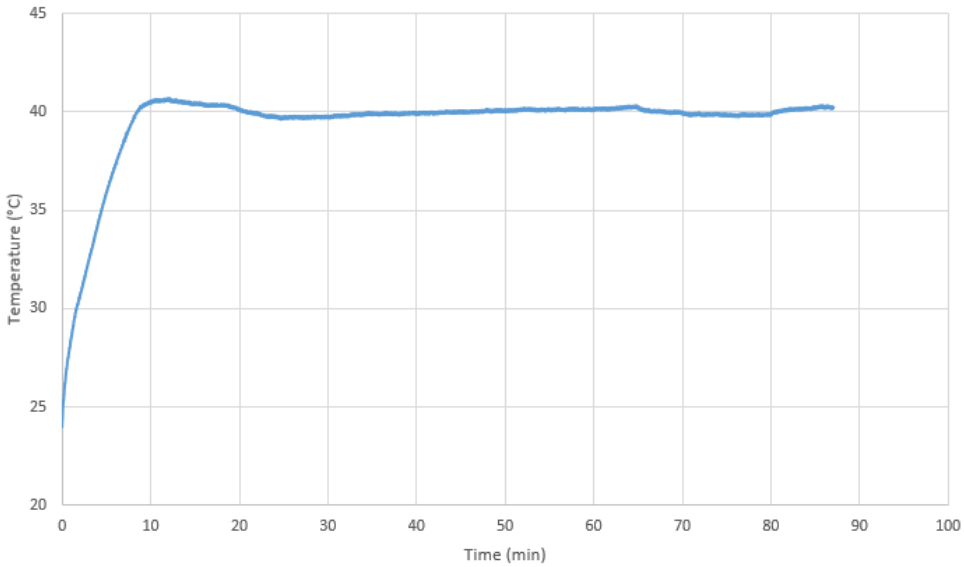

Figure 42: Temperature evolution at the sensors' location in the gas phase.

Thus, the H_2 sensor was periodically calibrated at 40 °C. As stated in the sensor's manual [58], 2 points with known H_2 concentration and voltage output values are necessary to perform the calibration. Indeed, a linear correlation exists between voltage output and

concentration, which is completely defined if two points are known.

One of the two points is simply the 0 point. A H_2 concentration of 0 μmol/L has been assumed for ambient air at 40 °C. The other point has been defined by using gas composed by 95% N_2 and 5% H_2. A volume was filled with the mentioned gas and simultaneously heated up to 40 °C. The H_2 concentration was found by applying the law of perfect gases:

$$p_{H_2} V = n_{H_2} RT \tag{7}$$

where p_{H_2} is the partial pressure of the hydrogen, V the volume occupied, n_{H_2} the amount of moles, R the gas constant and T the temperature. p_{H_2} is given by the total pressure of the gas, which is also sensed by the hydrogen sensor, multiplied times the molar fraction of hydrogen, i.e., 5%. From equation 7 it is possible to obtain an expression for the concentration of hydrogen at the described conditions:

$$\frac{n_{H_2}}{V} = \frac{p_{H_2}}{RT} \tag{8}$$

Table 4 reports the voltage outputs and the H_2 concentrations for a typical calibration. The calibration process was periodically repeated to ensure reliability of the measures.

Table 4: Hydrogen sensor's calibration points

H_2 Concentration (μmol/L)	Voltage (mV)
0	7.33
1975.83	272.76

Appendix 2: Estimation of $OH^\bullet$ radicals using TPA

As a first step towards the estimation of the concentration of $OH^\bullet$ radicals, a calibration was done to find a correlation between known concentrations of hTPA and the corresponding intensity of the fluorescent peak at 425 nm, consequent to excitation at 325 nm. The calibration is summarized in Figure 43, that shows a linear relation between concentration and intensity.

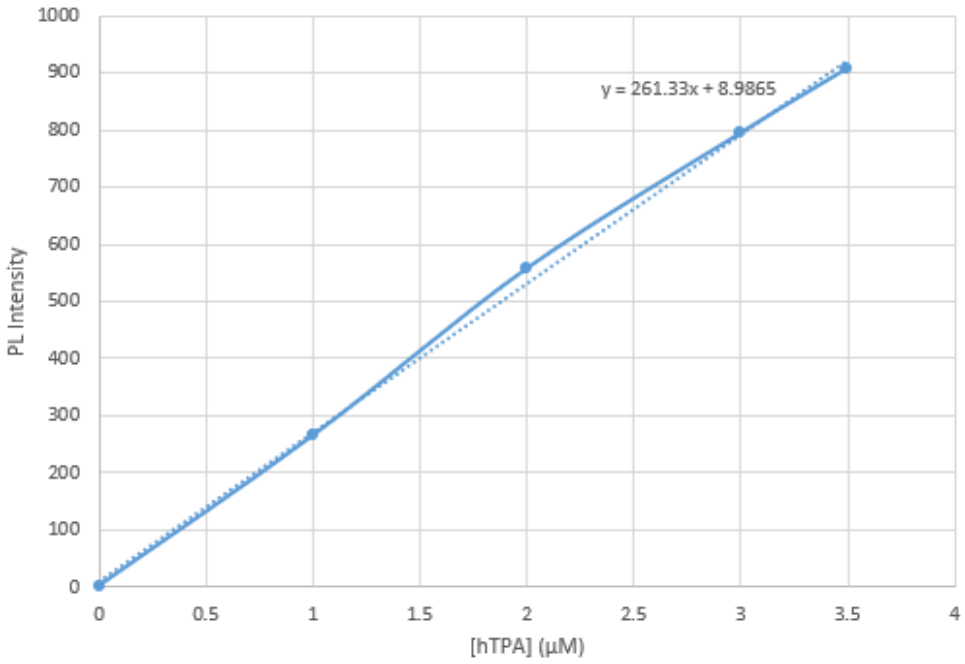

Figure 43: Relation between hTPA concentration and fluorescent intensity at 425 nm.

A linear interpolation of the calibrating points, whose equation is specified in the graph, allows to find an unknown concentration of hTPA given a certain fluorescent intensity. The intensity of the peak emission at 425 nm measured after the experiment with TiO_2/Pt 0.5 % described in Subsection 10.2 was equal to 341.8. This value, according to the calibration curve in Figure 43, corresponds to a hTPA concentration of 1.27 μM. Then, Equation 6 was applied to find the steady state concentration of $OH^\bullet$ radicals. In order to provide an accurate measure the quenching rate of hTPA should be taken into account, as hTPA can also react with $OH^\bullet$ radicals. However, being the concentration of hTPA much lower than that of TPA, the quenching rate has been considered negligible compared to the generation rate. Equation 6 was then the only equation applied. Considering the small irradiation time, a linear approximation has been performed, according to which Equation 6 can be re-written in the following form:

$$\frac{[hTPA]_{t_1} - [hTPA]_{t_0}}{t_1 - t_0} = k[TPA]_{ave}[OH^\bullet]_{ss}Y \tag{9}$$

t_0 represents the time instant at the beginning of the reaction, set equal to 0 s, while t_1 is the time instant associated to the end of the reaction and corresponding to 5 min. The hTPA concentration at t_1 has been obtained above, while it is equal to 0 at t_0. $[TPA]_{ave}$ represents the average concentration of TPA, calculated as the arithmetic average of the TPA concentrations at t_0 and t_1. The TPA concentration at t_0 is that of the original solution, i.e., 500 μM, while the concentration at t_1 can be found using the calculated

concentration of hTPA at t_1:

$$[TPA]_{t_1} = [TPA]_{t_0} - \frac{[hTPA]_{t_1}}{Y} \tag{10}$$

Where Y is the fraction of reacted TPA molecules that were converted to hTPA. The equation leads to a concentration of TPA at t_1 equal to 498.2 μM.
All the necessary values are thus known and the steady state concentration of $OH^{\bullet}$ radicals can be obtained.